

2008

ASSESSMENT OF TORNADO HAZARD MAPS FOR SOUTHERN ONTARIO

Li Tan
Western University

Follow this and additional works at: <https://ir.lib.uwo.ca/digitizedtheses>

Recommended Citation

Tan, Li, "ASSESSMENT OF TORNADO HAZARD MAPS FOR SOUTHERN ONTARIO" (2008). *Digitized Theses*. 4248.

<https://ir.lib.uwo.ca/digitizedtheses/4248>

This Thesis is brought to you for free and open access by the Digitized Special Collections at Scholarship@Western. It has been accepted for inclusion in Digitized Theses by an authorized administrator of Scholarship@Western. For more information, please contact wlsadmin@uwo.ca.

ASSESSMENT OF TORNADO HAZARD MAPS FOR SOUTHERN ONTARIO

(Thesis format: Integrated-Article)

by

Li Tan

Department of Civil and Environmental Engineering
Graduate Program in Engineering Science

Submitted in partial fulfillment of the
requirement for the degree of
Master of Engineering Science

School of Graduate and Postdoctoral Studies

The University of Western Ontario

London, Ontario

December, 2008

/

© Li Tan 2008

ABSTRACT

Probabilistic quantitative tornado hazard assessment is often based on the consideration that the spatial distribution of tornado occurrence is homogeneous in a region. While this assumption simplifies the analysis, it could over- and under- estimate tornado hazard for regions with lower and higher tornadic activity if an average rate of tornado occurrence is employed. The degree of over- and under-estimation is unknown. This study is focused on the assessment of the impact of spatial inhomogeneity of tornado occurrence on the estimated tornado hazard, and the development of tornado hazard maps for southern Ontario. The obtained results indicate that the tornado hazard at the factored design wind speed level is much smaller than the wind hazard due to synoptic winds even if the spatial inhomogeneity of tornado occurrence is considered. Furthermore, the results show that the spatial inhomogeneity of tornado occurrence has significant impact on the spatial tornado hazard level, that the return period values of tornado wind speed vary significantly over the considered region, and that the inhomogeneity must be considered in developing probabilistic quantitative tornado hazard maps.

Also, an attempt is made to assemble an approach for assessing the tornado hazard considering the uncertainty in the tornado occurrence rate in time and space. The quantification of this uncertainty is carried out by using the hierarchical Bayesian modeling and Markov Chain Monte Carlo technique. Results showed that it is feasible to use such an assembled approach to assess the tornado hazard maps, which incorporate the uncertainty in tornado occurrences.

ACKNOWLEDGEMENTS

I thank my supervisor Professor Hanping Hong for his continuous guidance, encouragement and advice throughout my graduate studies and the number of hours he spent with me on this research. It has been a privilege and a pleasure to work with a mentor with such wisdom and graciousness.

Constructive comments and suggestions by S. Banik are much appreciated. I thank all the friends that I have met over my many years at University of Western Ontario. I thank my thesis examiners for their constructive comments and suggestions.

Finally, a very special thanks to my farther, mother and brother for their love and support. This thesis is dedicated to my husband, Jun, who always has confidence in me and whose encouragement is essential for the completion of my thesis.

Table of Contents	Page
Certificate of Examination	ii
Abstract	iii
Acknowledgment	iv
Table of contents	v
List of Tables	vii
List of Figures	viii
Nomenclature	x
Chapter 1 Introduction	1
1.1 Background	1
1.2 Objectives and thesis outline	2
References	4
Chapter 2 Influence of spatial inhomogeneity of tornado occurrence on estimated tornado hazard contour maps for southern Ontario	6
2.1 Introduction	6
2.2 Wind hazard estimate with spatial inhomogeneity of tornado occurrence	8
2.2.1 Probabilistic model for tornado hazard assessment	8
2.2.2 Characteristics of tornado occurrence and path	11
2.2.3 Adopted probabilistic wind field model	17
2.3 Assessment of tornado hazard maps	20
2.3.1 Estimating tornado striking rate	20
2.3.2 Tornado hazard maps for southern Ontario	25
2.4 Conclusions	28
References	31
Chapter 3 Application of hierarchical Bayesian model for assessing tornado occurrence intensity and tornado hazard map for southern Ontario	35
3.1 Introduction	35
3.2 Tornado catalogue and empirical spatial occurrence	37

3.3 Bayesian estimate of tornado occurrence intensity	41
3.3.1 Hierarchical Bayesian model	41
3.3.2 Estimation of tornado occurrence intensity	48
3.4 Tornado hazard maps	54
3.4.1 Adopted formulation and probability distribution of tornado wind speed	54
3.4.2 Estimated tornado contour maps	55
3.5 Discussions and conclusions	58
References	60
Chapter 4 Conclusions and recommended future studies	63
4.1 Conclusions	63
4.2 Recommended future studies	64
Appendix A Adopted tornado wind field model	65
Vita	73

LIST OF TABLES

Table 2.1	Statistics of tornado occurrence for southern Ontario from 1950 to 1992.	12
Table 2.2a	Tornado path direction in Southern Ontario.	17
Table 2.2b	Distribution parameters for the tornado path length and width.	17
Table 3.1	Statistics of tornado occurrence for southern Ontario from 1950 to 1992.	38
Table 3.2	Summary of the adopted hierarchical Bayesian model.	45
Table 3.3	Summary of the assigned priors and estimated posteriors for the model parameters and hyperparameters.	46

LIST OF FIGURES

Figure 2.1	Confirmed and probable tornadoes for southern Ontario for the period 1950-1992.	11
Figure 2.2	Spatial distribution of the tornado occurrence intensity, $f_{\Lambda}(\lambda)$ for southern Ontario.	15
Figure 2.3	Illustration of tornado wind field model.	18
Figure 2.4	Probability distribution function of maximum tornado horizontal wind speed (3-second gust wind speed) for a randomly selected point within the striking area with intensity F_{Ai} .	19
Figure 2.5	Schematics illustrating tornado damage area for estimating the striking rate in southern Ontario	21
Figure 2.6	Spatial variation of the rate of striking for tornado with intensity F_{Ai} in southern Ontario.	22
Figure 2.7	Contour map of the ratios between the rate of striking with intensity F_{Ai} and the occurrence rate (r_{FAi}) for southern Ontario.	23
Figure 2.8	Contour map of the ratios between the rate of striking with intensity F_{Ai} and the occurrence rate (R_{FAi}) for southern Ontario.	24
Figure 2.9	Probability distribution function of maximum tornado wind speed: a) for Toronto Pearson International Airport, b) for London Airport.	26
Figure 2.10	Contour map of tornado wind speed: a) for return period of 10^5 years, b) for return period of 10^6 years, c) for return period of 10^7 years.	27
Figure 2.11	Contour map of exceedance probabilities for the maximum tornado wind speed equal to 304 (km/h).	28
Figure 3.1	Confirmed and probable tornadoes for southern Ontario for the period 1950-1992.	38
Figure 3.2	Tornado touchdown counts within selected regular grid cells based on tornado catalogue from 1950 to 1992: a) all tornados from 1950 to 1992 considering small grid cells; b) all tornados from 1985 to	39

1992 using large grid cells.

- Figure 3.3 Time series of all tornado reports in southern Ontario from 1950 to 1992. 40
- Figure 3.4 Illustration of samples of two chains considering $i=28$ and $t=4$: a) $\lambda(s_i; t)$, b) $p(s_i; t)$, c) $\varepsilon(s_i; t)$. 49
- Figure 3.5 Annual average posterior mean and standard deviation of $p(s_i, t)$: a) Mean, and b) Standard Deviation. 50
- Figure 3.6 Time series of the mean of $p(s_i, t)$ for cells representing the City of Toronto and the City of London. 51
- Figure 3.7 Posterior mean and standard deviation of $\beta(s_i)$: a) Mean, and b) Standard deviation. 52
- Figure 3.8 Annual average posterior mean and standard Deviation of $\eta(s_i; t)$: a) Mean, and b) Standard deviation. 52
- Figure 3.9 Annual average posterior mean and standard deviation of $\lambda(s_i; t)$: a) Mean and b) Standard deviation. 53
- Figure 3.10 Time series of the mean of $\lambda(s_i; t)$ at grid cells representing the city of Toronto and London. 53
- Figure 3.11 Probability distribution function of maximum tornado horizontal wind speed (3 second gust wind speed) for a randomly selected point within the striking area. 55
- Figure 3.12 Contour map of return period values of tornado wind speed for Cases 1 and 2: a) Case 1 with return period equal to 10^5 , b) Case 1 with return period equal to 10^6 , c) Case 2 with return period equal to 10^5 , d) Case 2 with return period equal to 10^6 . 57

NOMENCLATURE

IN CHAPTER 2:

- A = tornado origin area
- $E(\bullet)$ = mathematical expectation
- $f_A(a)$ = probability density function of A at a
- $f_\Lambda(\lambda)$ = probability density function of tornado occurrence intensity within an area of interest
- $F(\bullet)$ = cumulative distribution function
- F_{Ai} = i^{th} tornado striking intensity
- F_i = tornado intensity in i^{th} Fujita scale
- h = bandwidth representing the intensity of smoothing
- L = length of a tornado path
- $\min(\bullet)$ = minimum value
- n_E = total number of tornado events occurred within Ω_S and time interval of interest
- n_{\max} = maximum F -scale of interest
- N = number of tornadoes
- N_c = corrected number of tornadoes
- N_o = observed number of tornadoes
- $P(\bullet)$ = probability of the term inside the parenthesis
- $P(F_j)$ = relative frequencies of tornado intensities based on N_o
- $P''(F_j)$ = updated relative frequencies of tornado intensities adjusted for F -scale classification error analysis
- r_{FAi} = ratio between γ_{A_i} and $\Lambda f_\Lambda(\lambda)$
- R_{FAi} = ratio between γ_{A_i} and $\Lambda f_\Lambda(\lambda) A_{A_i}$
- s_i = i^{th} location a tornado event occurs at
- S = area of the reference region
- T = time period
- v = specified wind speed
- V = maximum gust wind speed in a tornado.

W	= tornado path width
γ	= rate of tornado striking a point of interest (within a considered region)
γ_{Ai}	= rate of tornado striking a point of interest (within a considered region) with striking intensity F_{Ai}
γ_i	= rate of tornado striking a point of interest with intensity F_i
γ_{Ci}	= rate of tornado classified as intensity F_i striking a point of interest (within a considered region)
$\lambda_i(s)$	= tornado occurrence intensity for tornadoes with intensity F_i at location s
$\hat{\lambda}_h(s)$	= estimate of the tornado occurrence intensity
Λ	= tornado occurrence rate of tornadoes within the considered area
Λ_i	= tornado occurrence rate of tornadoes classified as intensity F_i within the considered area
Ω	= domain of integration
Ω_S	= integration domain for the considered area with area S
$\ \bullet\ $	= Euclidean distance of the vector inside the parenthesis

IN CHAPTER 3:

a_1	= regressional parameter for $z_1(s_i)$
a_2	= regressional parameter for $z_2(s_i)$
diag[•]	= a diagonal matrix
$f_{IG}(x)$	= probability density function of inverse gamma distributions
$f_N(x)$	= probability density function of normal distributions
$f_U(x)$	= probability density function of uniform distributions
$f_\lambda(\lambda)$	= probability density function of tornado occurrence intensity within an area of interest
F_{Ai}	= i^{th} tornado striking intensity
F_i	= tornado intensity in i^{th} Fujita scale

- iid* = independent identical distributed
- IG(\bullet) = inverse Gamma distributions
- logit (\bullet) = logit function
- n = number of grid cells within considering region
- n_E = total number of tornado events occurred within a region and time interval of interest
- n_{\max} = maximum F-scale of interest
- N_c = corrected number of tornadoes
- N_o = observed number of tornadoes
- N(\bullet) = normal distributions
- $p(s_i; t)$ = non-zero-inflated Poisson probability that tornado count in grid-cell s_i time t follows a Poisson distribution
- p_t = $(p(s_1; t), \dots, p(s_n; t))'$, an $n \times 1$ vector representing the non-zero-inflated probabilities at time t
- $P(\bullet)$ = probability of the term inside the parenthesis
- $P''(F_j)$ = updated relative frequencies of tornado intensities adjusted for F -scale classification error analysis
- Pois(\bullet) = Poisson distributions
- r_{FAi} = ratio between γ_{A_j} and $\Lambda f_{\Lambda}(\lambda) A_{A_j}$
- R_{FAi} = ratio between γ_{A_j} and $\Lambda f_{\Lambda}(\lambda)$
- s_i = i^{th} grid cell a tornado event occurs at
- t = time index representing the t -th year of interest
- T = time period
- U(\bullet) = uniform distributions
- v = a specified wind speed.
- $v(s_i)$ = variable representing the spatial random effect in grid-cell s_i
- V = maximum gust wind speed in a tornado
- W = width of a tornado path
- x_t = $\{1, \dots, T\}$, representing a year index
- $Y(s_i; t)$ = variable representing the tornado report counts in grid-cell s_i at time t

- Y_t = $(Y(s_1;t), \dots, Y(s_n;t))'$, an $n \times 1$ vector representing the tornado report counts at time t
- $z_1(s_i)$ = dummy variable indicating whether the grid-cell s_i is located "data rich" region
- $z_2(s_i)$ = dummy variable indicating whether the grid-cell s_i is located "data poor" region
- α = $n \times 1$ vector of the discrete Fourier transform (DFT) operation on β
- β = $(\beta(s_1), \dots, \beta(s_n))'$, an $n \times 1$ vector representing the temporal trend
- γ_{Ai} = rate of tornado striking a point of interest (within a considered region) with striking intensity F_{Ai}
- $\gamma(s_i;t)$ = variable representing the error process for process p in grid-cell s_i , time t
- δ = $n \times 1$ vector representing the mean of vector ξ_t
- $\varepsilon(s_i;t)$ = variable representing the random effects in grid-cell s_i , time t
- ε_t = $(\varepsilon(s_1;t), \dots, \varepsilon(s_n;t))'$, an $n \times 1$ vector representing the random effects at time t
- $\eta(s_i;t)$ = variable representing the error process at grid-cell s_i , time t
- η_t = $(\eta(s_1;t), \dots, \eta(s_n;t))'$, an $n \times 1$ vector representing the the error process at time t
- θ = parameter of the exponential correlation function for the α process, representing the autocorrelation range
- θ_ξ = parameter of the exponential correlation function for the ξ_t process, representing the autocorrelation range
- $\lambda(s_i;t)$ = variable representing the Poisson mean in grid-cell s_i and time t
- λ_t = $(\lambda(s_1;t), \dots, \lambda(s_n;t))'$, an $n \times 1$ vector representing the Poisson mean at time t
- Λ = tornado occurrence rate of tornadoes within the considered area
- ξ_t = discrete Fourier transform (DFT) on vector η_t
- σ^2 = variance of vector α

- σ_v^2 = variance of variable $v(s_i)$
- σ_γ^2 = variance of variable $\gamma(s_i; t)$
- $\sigma_{\delta,1}^2$ = variance of variable $\delta(s_1)$
- $\sigma_{\delta,2}^2$ = variance of variable $\delta(s_i), (i = 2, \dots, n)$
- σ_ε^2 = variance of variable $\varepsilon(s_i; t)$
- σ_ξ^2 = variance of vector ξ_t
- $\Sigma_\alpha(\theta)$ = spatial correlation matrix of α
- $\Sigma_\xi(\theta_\xi)$ = spatial correlation matrix of ξ_t
- Φ = $n \times n$ matrix of Fourier basis functions
- Ω_S = integration domain for the considered area with area S
- $1'_{n-1}$ = $1 \times (n-1)$ vector of ones
- \sim = sign representing that the stochastic process or random variable on the left follows the right probabilistic distribution

CHAPTER 1

INTRODUCTION

1.1 Background

Tornadoes cause significant property damage and fatalities in North America. Applied Insurance Research (AIR 2008) report indicated that the annual average aggregated insured losses caused by severe thunderstorms, including tornadoes, are approximately equal to those due to hurricanes in recent years in North America. Although the annual number of tornado reports in Canada is far less than that in US (about 100 tornados per year occur in Canada), tornados are one of the most destructive natural hazards in terms of property damage and fatalities in the province of Ontario, Canada (Etkin 1999). Due to high concentration of population, infrastructure and structures in southern Ontario, it is desirable to assess the tornado hazard for this region.

The tornado occurrence process is uncertain. Probabilistic models, including the Poisson process, have been used in the literature to model this process (e.g., Wen and Chu 1973, Garson et al. 1975, Twisdale and Dunn 1983). Furthermore, although several tornado wind field models are available in the literature (see Nolan 2005, and Lewellen and Lewellen 2007), the physical-mathematical based models that can be used to describe the observed tornado damages and used to assess tornado hazard are very limited. One such model suitable for quantitative tornado hazard assessment is developed by Twisdale et al. (1981).

By ignoring the spatial inhomogeneity of tornado occurrence and adopting the probabilistic wind field model developed by Twisdale et al. (1981), Banik et al (2007, 2008) provided the first probabilistic quantitative tornado hazard assessment for a point,

line and spatially distributed structures in southern Ontario. While the consideration of spatially homogeneous tornado occurrence simplifies the numerical analysis, it could over- and under- estimate tornado hazard for regions with lower and higher tornadic activity if an average rate of tornado occurrence is employed. The degree of over- and under-estimation is unknown. Furthermore, the available tornado catalogue is relatively short, and there is statistical uncertainty associated with the tornado occurrence rate. The impact of this uncertainty on the estimated tornado hazard has not been quantified.

1.2 Objectives and thesis outline

The main objectives of the present study are to estimate tornado hazard for southern Ontario considering the influence of spatial inhomogeneity of tornado occurrence, to develop tornado hazard contour maps for the region under investigation, and to assess the impact of the uncertainty in tornado occurrence rate on the estimated tornado hazard.

The estimation of tornado hazard for southern Ontario with spatial inhomogeneity of tornado occurrence, and the development of tornado hazard contour maps for the region are documented in Chapter 2. For the analysis, the tornado catalogue described in Sills (2004) is employed, and the two-dimensional quartic kernel estimation technique (Bailey and Gatrell, 1995) is used to develop the nonhomogeneous tornado occurrence intensity. This developed tornado intensity is then used in assessing the tornado striking rate for sites of interest and combined with the probability distribution of tornado wind speed to assess the tornado hazard and tornado wind speed contour maps.

The investigation of the degree of uncertainty in the spatially varying tornado occurrence rate and its impact on the estimated tornado hazard is described in Chapter 3. For the assessment of uncertainty in the spatially varying tornado occurrence rate, the

hierarchical Bayesian spatiotemporal model developed by Wikle and Anderson (2003) is adopted. Chapter 3 is focused on the feasibility of such an assessment rather than provide a definitive evaluation of the uncertainty in the occurrence rate, and it is also focused on the sensitivity of the tornado hazard to such an uncertainty. In other words, the assembled approach is aimed at providing a basis for more detailed and extensive analysis leading to a definitive tornado hazard map in the future. Therefore, the tornado hazard map provided in Chapter 3 should not be used as a definitive recommendation for the tornado hazard maps.

Finally, in Chapter 4, a summary of conclusions of the thesis is given and, a few suggested future research topics are provided.

References

1. AIR. 2008. The Atlanta tornado. AIR Currents. Online publication by Applied Insurance Research, Boston, MA.
2. Bailey, T.C. and Gatrell, A.C. 1995. Interactive spatial data analysis. Longman Scientific and technical, London.
3. Banik, S.S., Hong, H.P. and Kopp, G.A. 2007. Tornado hazard assessment for southern Ontario. Canadian Journal of Civil Engineering, vol. 34, pp. 830-842.
4. Banik, S.S., Hong, H.P. and Kopp, G.A. 2008. Assessment of tornado hazard for spatially distributed systems in southern Ontario. Journal of Wind Engineering and Industrial Aerodynamics, vol. 96, pp. 1376-1389.
5. Etkin, D.A. 1999. Extreme events and natural disasters in an era of increasing environmental change. Report of Workshop on Emerging Environmental Issues in Ontario Environmental Monograph No.15. Institute for Environmental Studies, University of Toronto, pp. 19-22.
6. Garson, R.C., Morla-Catalan, J., and Cornell, C.A. 1975. Tornado design winds based on risks. ASCE Journal of the Structural division, 101, pp. 1883- 1897.
7. Lewellen, D.C. and Lewellen, W.S. 2007, Near-surface intensification of tornado vortices, Journal of Atmospheric Science, 64, 2176-2194.
8. Nolan, D.S. 2005, A New Scaling for Tornado-Like Vortices, Journal of Atmospheric Science, 62, 2639-2645.
9. Sills, D.M.L, Scriver, S.J. and King, P.W.S. 2004. The tornadoes in Ontario project (TOP). Preprints, 22nd AMS Conference on Severe Local Storms, Hyannis, MA, Amer. Meteorol. Soc., CD-ROM 7B.5.

10. Twisdale, L.A., Dunn, W.L., Horie, Y. and Davis, T.L. 1981. Tornado Missile Simulation and design methodology, Vol.2, Model verification and database updates, Report prepared by Research Triangle Institute, Research Triangle Park, North Carolina, August 1981.
11. Twisdale, L.A., and Dunn, W.L. 1983. Probabilistic analysis of tornado wind risks. ASCE Journal of the Structural division. 109, pp. 468-488.
12. Wen, Y.K. and Chu, S.L. 1973. Tornado risks and design wind speed. ASCE Journal of the Structural division, vol. 99, pp. 2409-2421.
13. Wikle, C.K. and Anderson, C.J. 2003. Climatological analysis of tornado report counts using a hierarchical Bayesian spatio-temporal model. Journal of Geophysical Research-Atmospheres, vol. 108, No. D24, 9005, doi: 10.1029/2002JD002806.

CHAPTER 2

INFLUENCE OF SPATIAL INHOMOGENEITY OF TORNADO OCCURRENCE ON ESTIMATED TORNADO HAZARD CONTOUR MAPS FOR SOUTHERN ONTARIO

2.1 Introduction

About 100 tornados per year occur in Canada and cause significant property damage and fatalities. The annual average aggregated insured losses caused by severe thunderstorms, including tornadoes, are approximately equal to those due to hurricanes in recent years in North America (AIR 2008). In fact, tornados are one of the most destructive natural hazards in terms of property damage and fatalities in the province of Ontario, Canada (Etkin 1999). The first systematic tornado database or historical tornado catalogue for Canada was established by Newark (1984). This database was subsequently improved and updated by Sills et al (2004) for Ontario. The information about the database includes indications on whether a recorded tornado event in the database is confirmed, probable and possible, the location and time of tornado occurrence, the tornado intensity in Fujita scale, and tornado path direction.

Recently, the historical tornado catalogue was employed by Banik et al. (2007, 2008) as the basis for estimating the tornado hazard and spatially distributed infrastructure systems for southern Ontario. These tornado hazard studies considered that the probabilistic tornado wind field can be modeled using the model advanced by Twisdale (1978), Dunn and Twisdale (1979) and Twisdale et al. (1981), and the spatial inhomogeneity of tornado occurrence can be ignored. The latter largely simplify the tornado hazard assessment for the considered region since the estimated tornado hazard

for a site or for a pair of sites are directly applicable for other sites within the southern Ontario region. The inhomogeneity of tornado occurrence for southern Ontario is recognized by many researchers, including Sills (1998), King et al. (2003) and Banik et al. (2007). Sills (1998) indicated that lake breeze boundary generated convection may be the dominant mechanism for storm formation and lead to a preferred southwest-to-northeast pattern of tornadic activity. However, the inhomogeneity of the tornado occurrence in southern Ontario has not been incorporated in estimating the quantitative tornado wind hazards or hazard maps. Furthermore, it is noted that meteorological type numerical simulations of tornado-like vortices have been presented in Nola and Farrell (1999), Nolan (2005), and Lewellen and Lewellen (2007), while Hangan and Kim (2006) developed a numerical model to represent the tornado wind field based on results of computational fluid dynamic simulations. However, none of these models is a probabilistic tornado wind field model that can be readily used for assessing tornado hazard.

The main objective of the present chapter is to estimate the tornado hazard for southern Ontario considering the influence of spatial inhomogeneity of tornado occurrence, and to develop tornado hazard contour maps for the region under investigation. For the assessment, similar to Banik et al (2007), the tornado wind field model developed by Twisdale et al. (1981) is adopted. To cope with the need to estimate tornado hazard for many locations, and to reduce the computing time, the hazard estimation is simplified by separating the analysis in two parts: assessment of tornado striking rate and probability distribution of maximum wind speed for a given tornado striking intensity. Details of the analysis procedure and model as well as numerical

results are provided in the following sections.

2.2 Wind hazard estimate with spatial inhomogeneity of tornado occurrence

2.2.1 Probabilistic model for tornado hazard assessment

Probabilistic model for tornado hazard assessment has been presented in the literature (e.g., Wen and Chu 1973; Garson et al. 1975; Twisdale et al. 1981, Banik et al. 2007) by assuming that the tornado occurrence is homogeneous in space, which simplifies the assessment for a region of interest. Furthermore, by assuming that the tornado occurrence in time follows a Poisson process and that the peak wind velocity for each tornado is independent and identically distributed, the probability that the maximum wind velocity due to tornado, V , exceeds a specified value v in a time period T (years) for a point of interest, $P_T(V > v)$, is given by (Wen and Chu 1973),

$$P_T(V > v) = 1 - \exp(-\gamma P(V > v)T) \quad (2.1)$$

where γ is the annual rate of tornado striking the point of interest for the tornados originated from a region with area S) and $P(V > v)$ represents the exceedance probability distribution of maximum wind speed of the tornado that strikes the point of interest.

$P(V > v)$ can be expressed as,

$$P(V > v) = \sum_{i=0}^{n_{\max}} P(V > v | F_i) P(F_i) \quad (2.2)$$

where F_i ($i = 0, \dots, n_{\max}$) represents the tornado with the i -th Fujita scale (F -scale) intensity; n_{\max} represents the maximum F -scale of interest; $P(V > v | F_i)$ is the probability that V is greater than v conditioned on that the tornado with the i -th Fujita scale strikes the point of interest; and $P(F_i)$ is the probability that the tornado with intensity F_i strikes the

point of interest. Alternatively, to simplify the analysis and to facilitate the incorporation of the uncertainty in the occurrence rate for each F -scale intensity tornados, Twisdale and Dunn (1983) proposed that $P_T(V > v)$ can be approximated by,

$$P_T(V > v) \approx \sum_{i=0}^{n_{\max}} (1 - \exp(-\gamma_{Ci} P(V > v | F_i) T)) \quad (2.3a)$$

where γ_{Ci} is the annual rate of tornado that is classified as F_i tornado and strikes the point of interest. It must be emphasized that in the above equation, F_i represents intensity of a tornado according to the classification. However, for a tornado classified as F_i tornado, its actual intensity varies along its path length as the friction of the ground dissipates the energy, and only a percentage of its path length (or damage area) is actually experiencing a tornado with intensity F_i , while the remaining portion of the path length experiences an intensity less than F_i (Twisdale et al. 1981). To distinguish the classified intensity and experienced intensity, we use F_{Ai} denotes the actually experienced (striking) tornado intensity by the portion of path length if the whole considered portion of path length experienced tornado of intensity F_i . If the probability that V is greater than v conditioned on the striking intensity F_{Ai} , $P(V > v | F_{Ai})$, is employed, Eq. (2.3a) becomes,

$$P_T(V > v) \approx \sum_{i=0}^{n_{\max}} (1 - \exp(-\gamma_{Ai} P(V > v | F_{Ai}) T)) \quad (2.3b)$$

where γ_{Ai} is the annual rate of tornado striking the point of interest with striking intensity F_{Ai} . This equation is used for the numerical analyses shown in the present study.

Note that a tornado is defined by its path length and width, and that $P(V > v | F_i)$ needs to be evaluated for Eq. (2.2), or Eq. (2.3a). If the tornado occurrence is homogeneous in space, $P(V > v | F_i)$ can be approximated by (Thom 1963),

$$P(V > v | F_i) = \int_{\Omega} \min(1, a/S) f_A(a) da \approx \min(1, E(A)/S) \quad (2.4)$$

where a is a value of A denoting the area of the origin of the tornados classified as intensity F_i that will strike a point of interest with $V > v$; $f_A(a)$ denotes the probability density distribution of A ; Ω denotes the domain of integration; and $E(\bullet)$ represents the mathematical expectation.

However, Eq. (2.4) is not applicable if the tornado occurrence is spatially inhomogeneous. This inhomogeneity is shown in Figure 2.1 by using the historical tornado catalogue for southern Ontario given by Sills et al. (2004). Use of the historical data in assessing the non-homogeneous spatial tornado occurrence rate will be discussed shortly. To take the inhomogeneity into account, consider, for the moment, that the spatial dependence of the tornado occurrence intensity (i.e., the number of tornado touchdowns per unit area per year), $\lambda_i(s)$, for tornados with intensity F_i is already estimated from the historical tornado catalogue, and that the probability density function of tornado occurrence intensity within an area of interest for tornado with intensity F_i , $f_{\Lambda_i}(\lambda_i)$, can be expressed as,

$$f_{\Lambda_i}(\lambda_i(s)) = \lambda_i(s) / \Lambda_i \quad (2.5)$$

where $\Lambda_i = \int_{\Omega_s} \lambda_i(s) ds$ represents the tornado occurrence rate of tornadoes classified as intensity F_i within the considered region, Ω_s represents the integration domain for the considered region, and s denotes a point within the domain.

Note that the tornado occurrence rate is not equal to the rate of tornado striking a point of interest, since the evaluation of the tornado striking rate for a tornado must consider the non-uniform tornado occurrence in space (within the considered region), the

variation of striking intensity, the path direction and the damage area. Furthermore, no simple analytical solution for evaluating γ_{Aj} is available and, as explained in the following, simple simulation technique can be used for its evaluation.

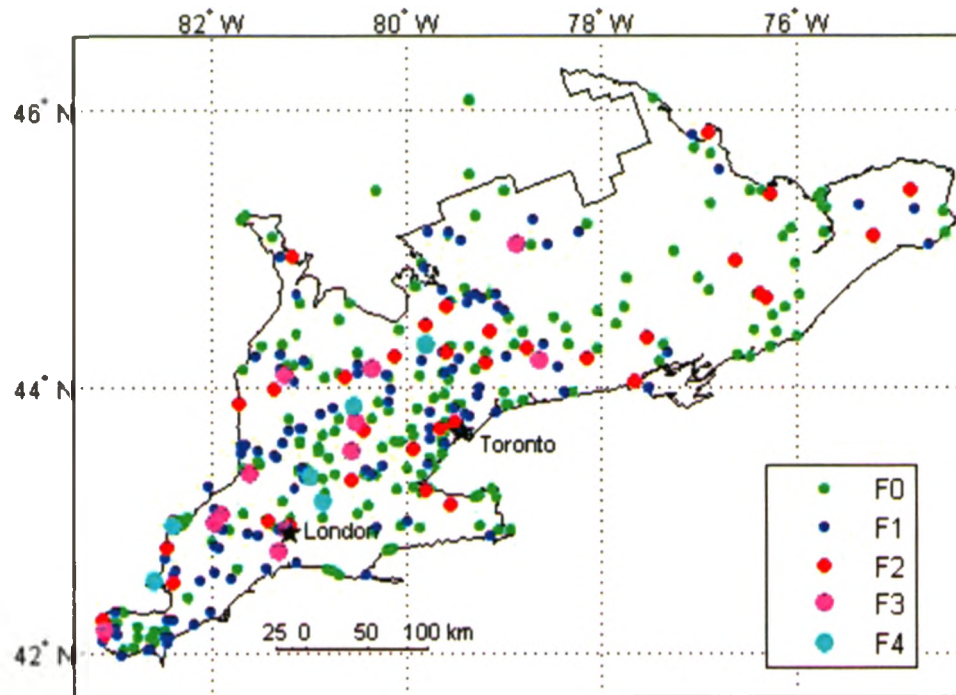


Figure 2.1 Confirmed and probable tornados for southern Ontario for the period 1950-1992.

2.2.2 Characteristics of tornado occurrence and path

The spatial inhomogeneity affects the estimated tornado hazard at a point, and especially the tornado hazard map for a geographic region. To assess this inhomogeneity, we note that the tornado database for Ontario developed by Newark (1984) and subsequently updated by Sills et al. (2004) includes information on the essential variables for many tornados. These variables include tornado intensity in *F*-scale, tornado occurrence time, geographic location of recorded tornado touchdown point, tornado direction of motion, tornado path length and whether the recorded tornado is identified as a confirmed, probable and possible tornado event. The confirmed category is defined so

that events are considered as tornados due to visual evidence or damage reports. The probable category includes events where all available evidence pointed to the likelihood of tornados. The possible category is used to define events where the tornado evidence is either ambiguous or unreliable. Sills et al. (2004) concluded that only confirmed and probable events provide the best representation of actual tornado touchdowns, because some non-tornadic events were potentially involved in the possible category. Hence, all tornado events, which were rated as either confirmed or probable and occurred in southern Ontario between the year 1950 and 1992, will be considered in this study. This time interval is chosen to be consistent with that of the tornado database of Ontario's neighbouring regions (i.e., Michigan, Ohio, Pennsylvania and New York State) in the United States, since some of the tornado's characteristics, which are not available in Ontario tornado database and are needed for tornado hazard assessment, can be obtained from the tornado database of the neighbouring regions.

Table 2.1. Statistics of tornado occurrence for southern Ontario from 1950 to 1992.

F -scale	F -scale wind speed range (km/h)	N_o	N_c	$P(F_j)$	$P''(F_j)$
F_0	64-116	196	280	0.5429	0.4425
F_1	117-165	110	157	0.3047	0.3101
F_2	166-216	37	37	0.1025	0.1620
F_3	217-269	12	12	0.0332	0.0567
F_4	270-335	6	6	0.0166	0.0230
F_5	336-446	0	0	0	0.0057
Total		361	492	1	1

Note that the reported tornado information on the tornado database does not reflect the actual historical tornado activities due to a) improved storm tracking and reporting network and possible increased number of witnesses of tornados (because of increased population density); and b) errors and bias in F -scale assignment during tornado reporting

process. Banik et al. (2007) carried out statistical analysis for tornados occurred in southern Ontario and in the neighbouring regions by considering both the de-trending (McDonald et al. 1975, Sigal et al. 2000) and error and bias correction (Twisdale et al. 1981). Such an analysis is carried out again since the selected region shown in Figure 2.1 for this study differs from that considered by Banik et al. (2007). The obtained results for the former are shown in Table 2.1, which are in close agreement to those given in the latter.

In Table 1, the ranges of the updated wind speed (fastest quarter mile gust winds) for each tornado intensity category proposed by Twisdale et al. (1981), which is to be used in the present study, are presented. N_o represents the observed number of tornados for each tornado intensity category; N_c represents the corrected number of tornados for each tornado intensity category; $P(F_j)$ represents the relative frequencies of tornado occurrence for each intensity F_j calculated directly based on N_o ; and $P''(F_j)$ ($j = 0, \dots, 5$) represents the updated relative frequencies of tornado intensities adjusted for F -scale classification error analysis (Twisdale et al. 1981). By considering the correction and adjustment, the updated occurrence rate of tornado with intensity F_i for southern Ontario, Λ_i per year equals $(492/43) \times P''(F_j)$.

Sills (1998), King et al. (2003) and Banik et al. (2007) pointed out that the tornado occurrences in southern Ontario are inhomogeneous in space. To further assess the spatial tornado occurrence pattern, and to obtain an estimate of spatially smoothed tornado occurrence rate over southern Ontario, two-dimensional quartic kernel estimation technique (Bailey and Gatrell, 1995) was considered. The technique provides a nonparametric estimate of the mean number of events per unit area for a set of regular

grid points. It estimates the tornado occurrence intensity at each grid point from the contribution of events per unit area within the ‘window’ centered on the grid point. More specifically, given the tornado historical catalogue containing n tornado events occurred (i.e., touchdowns) at locations s_1, \dots, s_n , an estimate of the tornado occurrence intensity at a grid point or location s denoted by $\hat{\lambda}_h(s)$, is obtained using (Bailey and Gatrell, 1995),

$$\hat{\lambda}_h(s) = \sum_{\|s-s_i\| < h} \frac{3}{\pi h^2} \left(1 - \frac{\|s-s_i\|^2}{h^2} \right) \quad (2.6)$$

where $\|s-s_i\|$ denotes the distance between the location s and the location of the i -th observed event s_i , and h denotes the bandwidth (i.e., the radius of the circular ‘window’) and determines the intensity of smoothing. The smoothness is directly proportional to the bandwidth; small bandwidth value retains more local features but exhibit spikes centered on the s_i . Bailey and Gatrell (1995) suggested that for a region with unit area, $h = 0.68n^{-0.2}$ could be used for estimating the intensity where n is the number of observed events in this region.

Note that if the number of the observed tornados for each tornado intensity category is large, estimates $\hat{\lambda}_h(s)$ for each tornado intensity category can be carried out directly. However, as the tornado intensity increases, the number of observed events becomes very scarce as shown in Table 2.1. Consequently, such an approach is inadequate if the estimates $\hat{\lambda}_h(s)$ for tornados with intensity greater than F_1 are of interest since there are only less than 40 tornados of categories F_2 to F_5 for the considered region. To overcome this problem, it is assumed that the spatial tornado occurrence intensity is independent of the tornado intensity, which allows the estimation of the spatial distribution of the tornado occurrence by using all tornado events in the historical tornado catalogue. By

adopting this assumption, and using the quartic kernel estimation technique with $h = 0.68n^{-0.2}$, the estimation of tornado occurrence intensity $\hat{\lambda}_h(s)$ using the historical tornado catalogue for southern Ontario for the period from 1950 to 1992 is carried out. By using this estimate and considering that the probability density function of tornado occurrence intensity $f_\Lambda(\lambda)$ is proportional to $\hat{\lambda}_h(s)$, the obtained $f_\Lambda(\lambda)$ is shown in Figure 2.2. Note that since $\hat{\lambda}_h(s)$ is spatially non-uniform, $f_\Lambda(\lambda)$ varies spatially as well. In other words, the tornado occurrence intensity in southern Ontario is not uniformly distributed over the considered region.

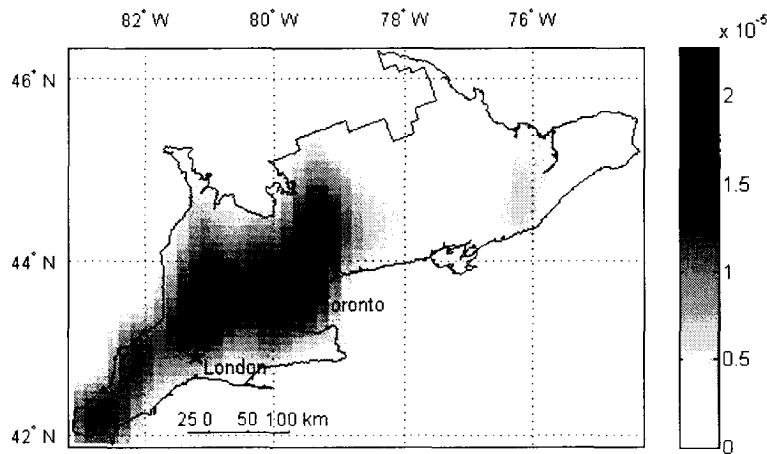


Figure 2.2 Spatial distribution of the tornado occurrence intensity, $f_\Lambda(\lambda)$ for southern Ontario.

Note that since the spatial occurrence is assumed to be independent of tornado intensity, $f_{\Lambda_i}(\lambda_i)$ ($i = 0, \dots, 5$) equals $f_\Lambda(\lambda)$ shown in Figure 2.2. Note also that to estimate the tornado striking rate, the obtained spatial distribution of tornado occurrence need to be adjusted for both the correction to the number of tornados and the

classification error as shown in Table 2.1.

Other statistical characteristics of tornados that are needed to assess the rate of tornado striking a point of interest, γ_{Ai} , are the tornado path direction, path length and path width. For practical purpose, the tornado path direction is considered to be the same for different F_i , and the tornado damage area could be modeled by a rectangle defined by the tornado length L and tornado width W (Twisdale et al. 1981). Since insufficient information is available in the tornado catalogue for southern Ontario to assess the statistics of the path direction, L and W , the probabilistic models developed by Banik et al. (2007) based on the tornado database of the neighbouring region of southern Ontario are adopted in the present study. Their study suggested that the tornado path direction can be modeled using the probability mass function shown in Table 2.2a, and the tornado length and tornado width can be modeled using the truncated Weibull distribution,

$$F(X < x) = \frac{1 - \exp(-ax^b)}{1 - \exp(-ac^b)}, \quad 0 < x \leq c \quad (2.7)$$

where X represents W (m) or L (km); a and b , which are shown in Table 2.2b for easy reference, are the scale and shape parameter of the probability distribution, respectively; and c is taken to be the maximum possible values for tornado length and width suggested by Fujita and Pearson (1973), which equals 504 km for the length and 4960 m for the width.

One more point that needs to be mentioned is that due to energy dissipation, the intensity of tornado varies along the tornado path length (Twisdale et al. 1981). This variation has been confirmed by observing tornado damage characteristics and photograph of life cycle features of many tornadoes; a probabilistic model defining the percentage of path length of striking intensity F_{Aj} ($j=1, \dots, i$) given that the tornado is

classified as intensity F_i is reported by Twisdale et al. (1981). This variation is essential in assessing the rate of tornado striking with striking intensity F_{Ai} .

Table 2.2a. Tornado path direction in southern Ontario (Banik et al. 2007).

Direction	N	NE	E	SE	S	SW	W	NW
Frequency	0.0422	0.378	0.4488	0.1084	0.0075	0.003	0.0015	0.0106

Table 2.2b. Distribution parameters for the tornado path length and width (Banik et al. 2007).

F -scale	Length		Width	
	a	b	a	b
F_0	0.9150	0.6442	0.0450	0.8812
F_1	0.5015	0.6618	0.0229	0.9147
F_2	0.2965	0.6563	0.0223	0.8124
F_3	0.0786	0.8282	0.0022	1.1271
F_4	0.0264	0.9865	0.0028	0.9591
F_5	0.0005	1.8758	1.18E-10	3.6684

2.2.3 Adopted probabilistic wind field model

A tornado wind field model is needed for a quantitative tornado wind hazard assessment. Some of the existing tornado wind field models used in the civil engineering literature can be classified as empirical model, experimental model or theoretical model. These models are developed based on investigation of historical tornado events (Hoecker 1960, 1961), laboratory experimental results (Ying and Chang 1970, Ward 1972) which are limited by the size and flow field of the experiment, and theoretical investigation considering axisymmetric flows in incompressible fluids (Kuo 1970, Wen 1975). However, none of these mentioned studies explicitly describes the variation of both wind speed components in a given tornado and wind field characteristics among different tornados in sizes and intensities. To overcome this and based on these models, a steady state model (along the tornado path length) proposed by Twisdale et al. (1981) and Dunn and Twisdale (1979) can be considered. This model is illustrated in Figure 3. It depends

on a set of model parameters: the ratio of the radial velocity to tangential velocity; the radius to the maximum tangential velocity at a reference height; the linear variation of the reference radius with height; the reference boundary layer thickness; the reference rotational velocity; the translational speed; and the tornado width. The model aims at approximating the variations of the vertical and horizontal wind speed across the tornado path width, and the probabilistic model parameters account for the natural variability observed among tornados, including tornado intensity, path length and width, translational speed, core radius, ratio of radial-to tangential wind speed components, core radius and boundary layer thickness. Mathematical details of this wind field model can be found in Twisdale et al. (1981) and in Dunn and Twisdale (1979) (see also Appendix A).

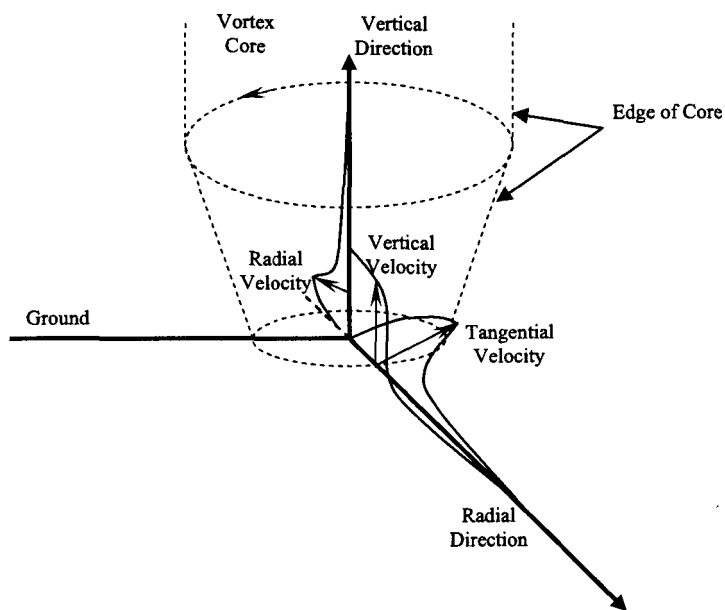


Figure 2.3. Illustration of tornado wind field model.

By adopting this model, probability distribution of the maximum horizontal wind speed V can be assessed for a randomly selected point at 10 m height and within a

tornado damage path. In this study, the assessment is carried out using simple simulation

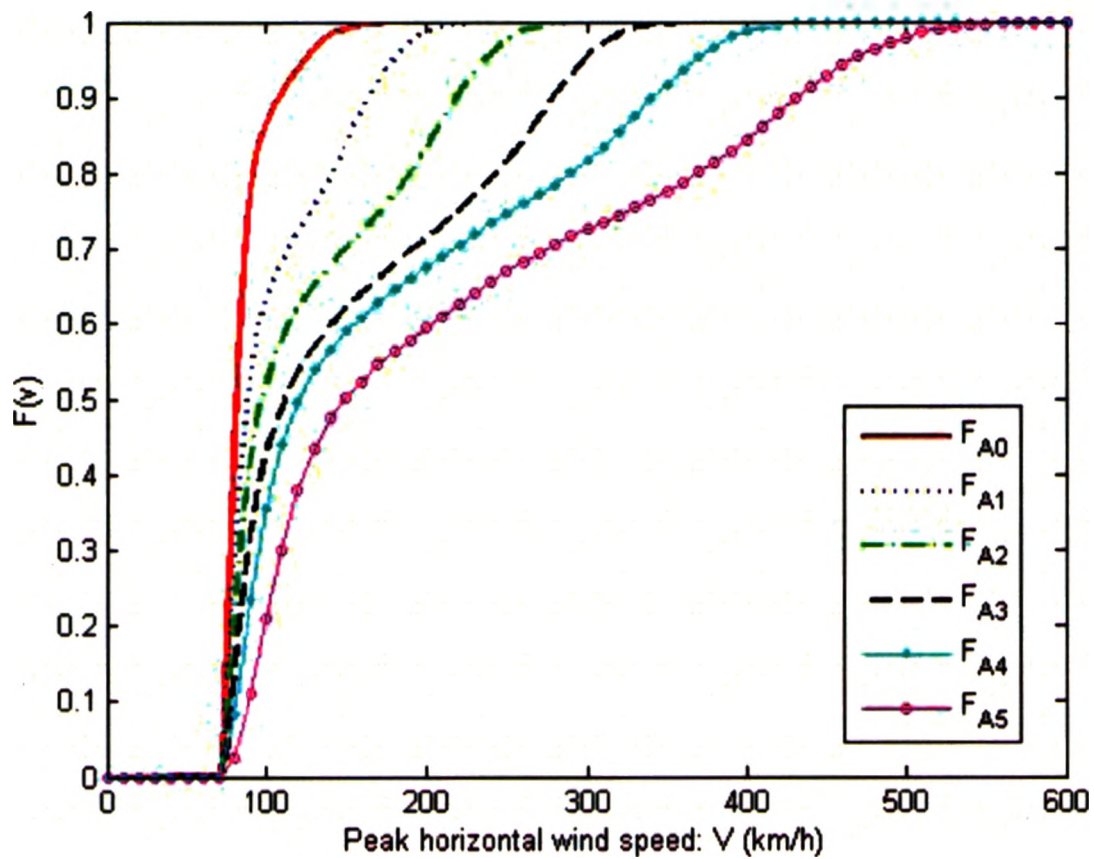


Figure 2.4. Probability distribution function of maximum tornado horizontal wind speed (3-second gust wind speed) for a randomly selected point within the striking area with intensity F_{Ai} .

technique. Given a tornado of intensity F_i , it basically consists of sampling the tornado intensity and path width, sampling the wind field model parameters, sampling a point within the tornado damage path with striking intensity F_{Ai} , and evaluating the maximum horizontal wind speed for the sampled point using the adopted wind field model. By carrying out this simulation, the obtained samples are used to form the probability distribution function of the maximum horizontal wind speed $P(V < v | F_{Ai})$ as shown in Figure 2.4. Note that conversion factors obtained from the curve given by Durst (1960) are used to estimate 3-second gust wind speed from other types of wind speed. The results presented in the figure indicate that as the striking intensity F_{Ai} increases the probability distribution function is shifted horizontally toward higher wind speed region,

which is expected. For moderate and low exceedance probability levels, the shift is about 50 km/hr, which approximately equals the increase in the mean wind speed between two consecutive F -scale tornado intensities shown in Table 2.1.

2.3 Assessment of tornado contour maps

2.3.1 Estimating the rate of tornado striking

As mentioned previously, no analytical solution for evaluating γ_{Aj} is available, so simple simulation technique is used for its estimation. In particular, to develop tornado wind speed contour maps or tornado hazard maps, the estimation of the tornado striking rate γ_{Aj} for a set of regular grid points covering southern Ontario as illustrated in Figure 2.5 is needed. The basic steps for evaluating γ_{Aj} (tornado strikes/year) are as follows:

- 1) Sample tornado touchdown site (i.e., tornado origin) according to the probability distribution of tornado occurrence (spatial) intensity, $f_{\Lambda}(\lambda)$;
- 2) Sample the tornado intensity according to $P''(F_i)$ ($i = 0, \dots, 5$) shown in Table 2.1;
- 3) Sample the tornado path direction, length and width based on the probabilistic models mentioned in the previous sections;
- 4) Sample the percentage of the path length whose striking intensity within the path length is F_{Aj} according to the tornado intensity variation along the tornado path length given by Twisdale et al. (1981);
- 5) Superimpose the tornado damage area on the region of interest illustrated in Figure 2.5 and check whether a grid point is within the tornado damage area within intensity F_{Aj} ; and
- 6) Repeating 1) and 5) n_E times to estimate γ_{Aj} for all the considered grid points where n_E

is the total number of tornado events occurred within Ω_S and time interval of interest.

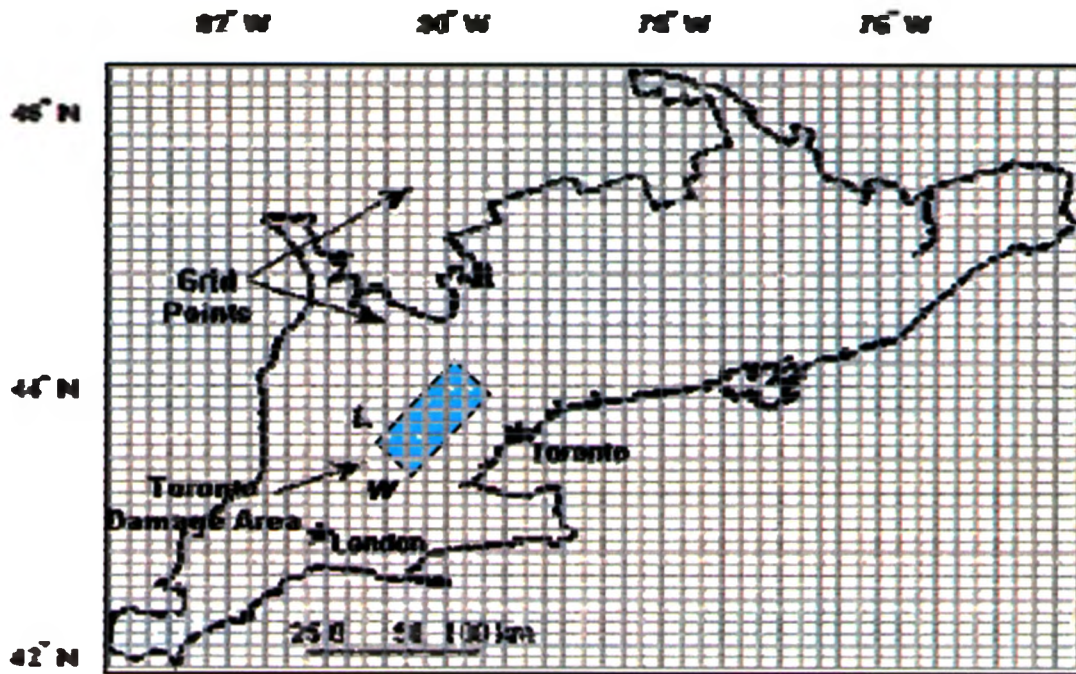


Figure 2.5 Schematics illustrating tornado damage area for estimating the striking rate in southern Ontario

Note that the above procedure is applicable to any region of interest. Note also that for the southern Ontario region, the average annual tornado occurrence rate, which equals 11.44 ($=492/43$) by considering the corrected number of tornados shown in Table 2.1, should be employed. By using the above procedure, the obtained tornado striking rate for southern Ontario is presented in Figure 2.6. For the results shown in Figure 2.6, a set of regular squared defined by 600×600 grid points is employed, and n_E equal to 100,000 was considered, which represents approximately 8740 years of simulated tornado activity.

Comparison of the results shown in Figures 2.2 and 2.6 indicates that the rate of striking with intensity F_{Ai} ($i = 1, \dots, 5$) follows similar trend as that of $f_{\Lambda}(\lambda)$. To better appreciate the relation between the striking rate and the occurrence intensity and to possibly develop a simple approximate approach in estimate the striking rate, ratios between γ_{Aj} and $\Lambda f_{\Lambda}(\lambda)$, defined by $r_{F_{Ai}}$, where $\Lambda = 492/43$, are calculated and shown in

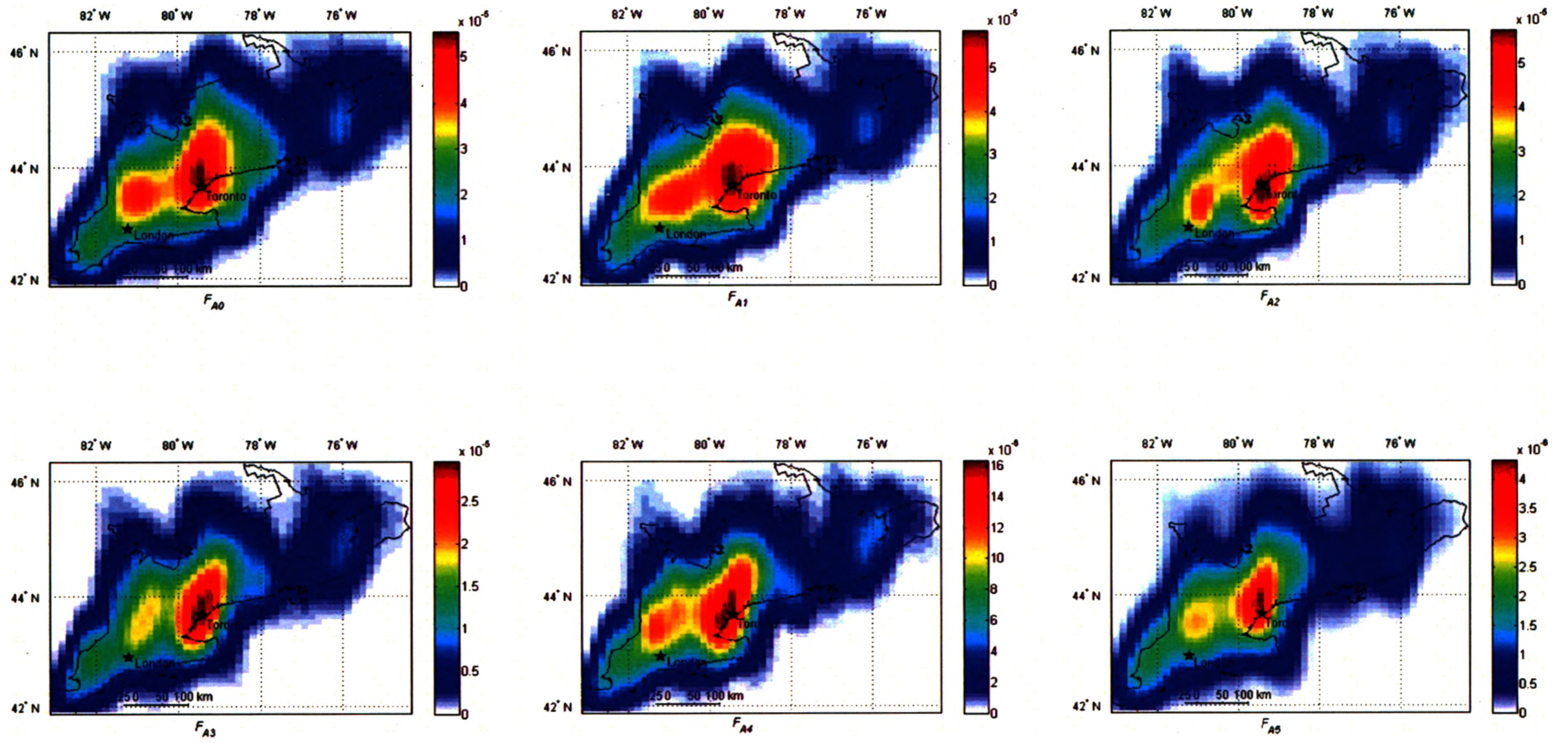


Figure 2.6 Spatial variation of the rate of striking for tornado with intensity F_{Ai} in southern Ontario

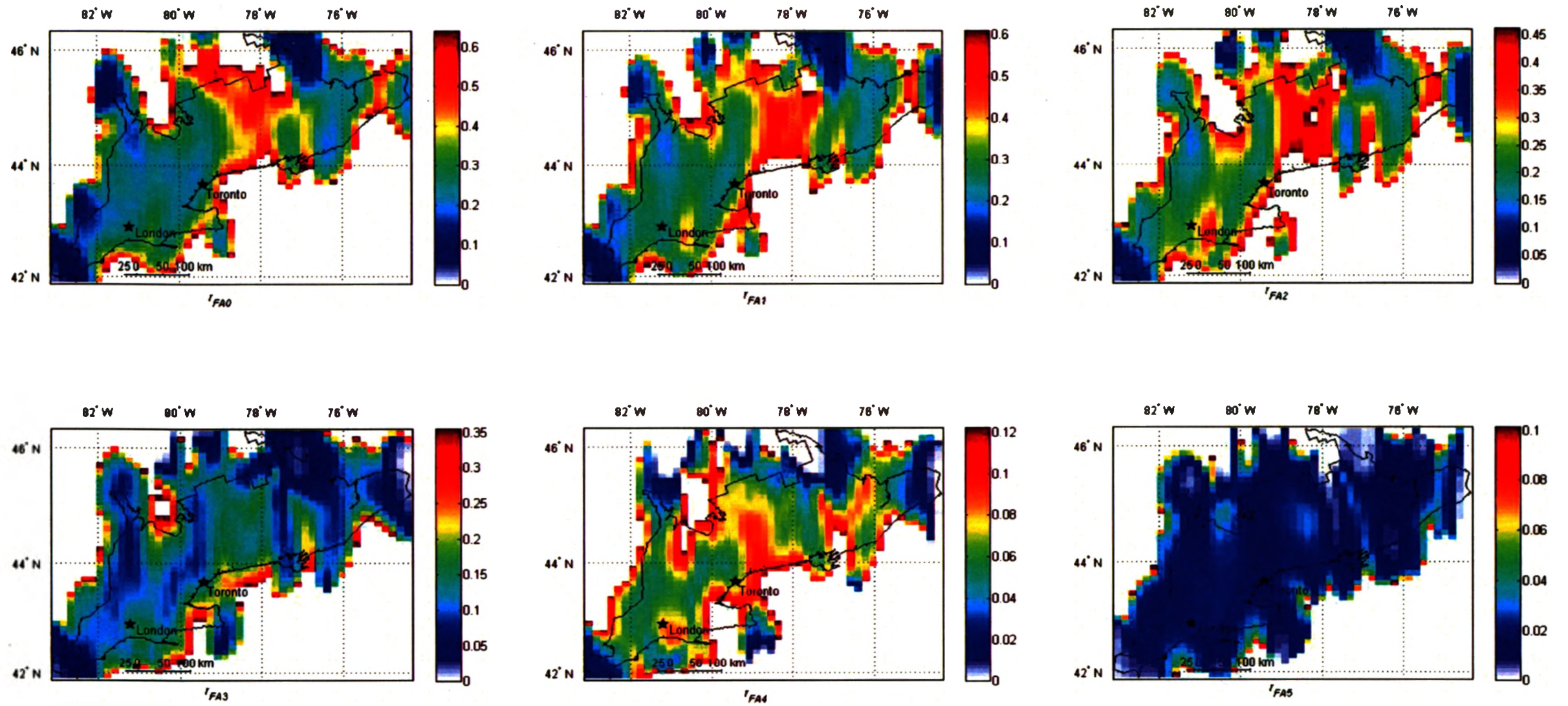


Figure 2.7 Contour map of the ratios between the rate of striking with intensity F_{Ai} and the occurrence intensity, r_{FAi} , in southern Ontario.

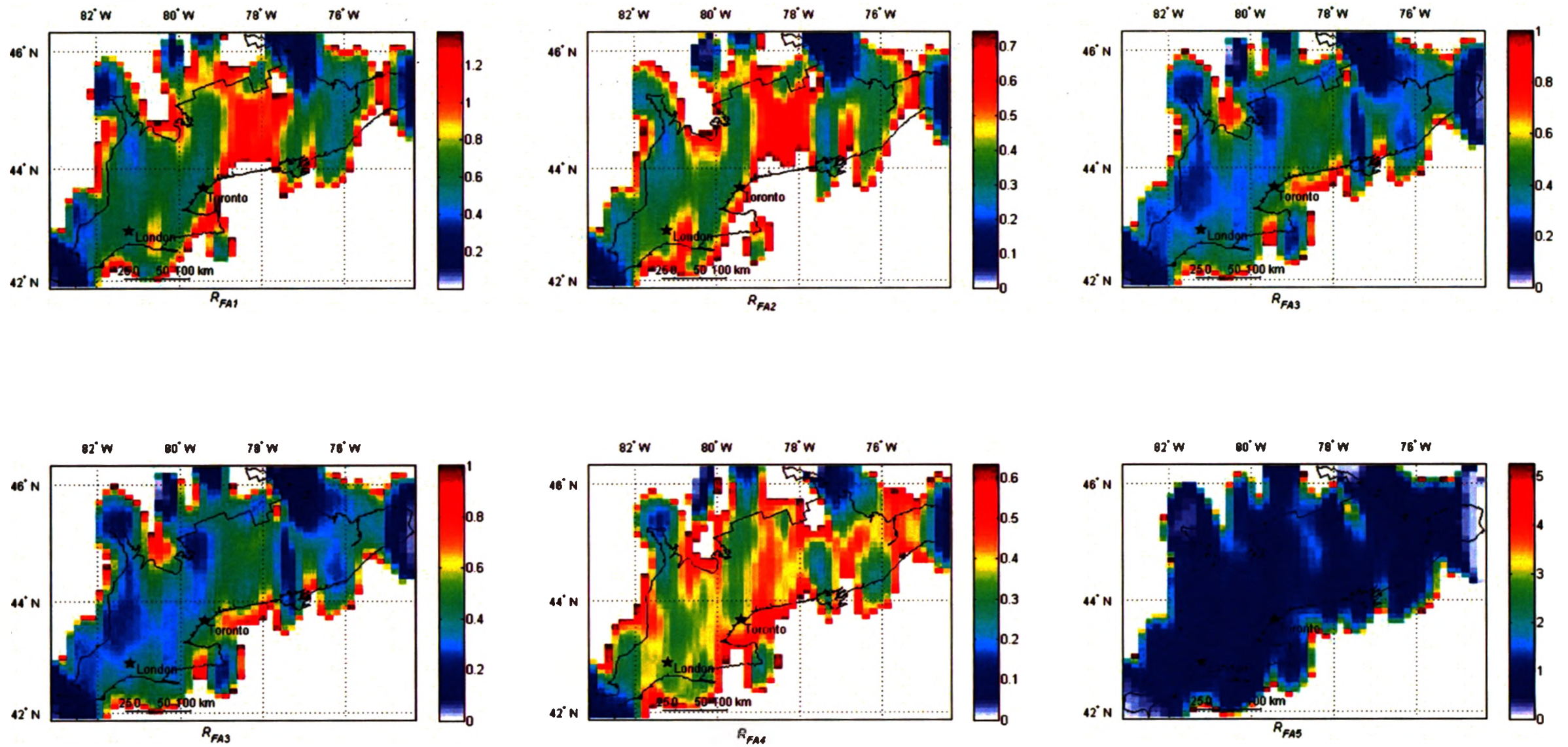


Figure 2.8. Contour map of the ratios between the rate of striking with intensity F_{Ai} and $\Lambda f_{\Lambda}(\lambda)P''(F_j)A_{Aj}$, R_{FAi} , in southern Ontario.

Figure 2.7. In particular, the ratios of γ_{Aj} to $\Lambda f_{\Lambda}(\lambda)$ ($j = 1, \dots, 5$) for Toronto Pearson International airport are respectively equal to 0.3378, 0.3970, 0.4312, 0.1740, 0.0883 and 0.0211. For London International airport, these ratios are respectively equal to 0.2059, 0.2777, 0.226, 0.0948, 0.0741 and 0.0168. Note that although the ratio is relatively uniform over the considered region, it can only be treated very approximately as a constant.

Furthermore, evaluation of the ratio of γ_{Aj} to $\Lambda f_{\Lambda}(\lambda) P''(F_j) A_{Aj}$, R_{FAi} , where A_{Aj} denotes the average tornado striking area with striking intensity F_{Aj} (i.e., the product of mean tornado length and width with intensity F_{Aj} derived from Table 2.2b) was carried out. The obtained results, which are the same as those shown in Figure 2.8 except scaling constants, again show that the ratio can only be treated very approximately as a constant for the considered region.

2.3.2 Tornado contour map for southern Ontario

To assess the contour map of tornado hazard, first, consider a particular grid point located at 43.3931°N and 79.3590°W , representing approximately the location of Toronto Pearson International Airport. For this grid point, we obtain the striking rate γ_{Ai} from Figure 2.6, which equals 4.39×10^{-5} , 5.16×10^{-5} , 5.61×10^{-5} , 2.26×10^{-5} , 1.15×10^{-5} and 2.23×10^{-6} .

Substituting these values and $P(V < v | F_{Ai})$ shown in Figure 2.4 into Eq. (2.3b), the estimated annual probability of exceedance function $P_T(V > v)$ is depicted in Figure 2.9a, which can be used to estimate the return period values. For example, the estimated return period values of the maximum tornado wind speed are 244 (km/h) for T equal to 10^5

years and 368 (km/h) for T equal to 10^6 years. To compare the tornado wind hazard to that of the synoptic wind hazard, a plot of the Gumbel distribution function fitted to annual maximum (synoptic) wind speed data is also shown in the same figure, and the factored design wind speed (i.e., value obtained by multiplying the 50-year return period value by $\sqrt{1.4}$, where 1.4 is the wind load factor suggested in NBCC (2005)) is identified in the figure as well. The figure shows that the tornado hazard at the factored design wind speed level is much smaller than the wind hazard due to synoptic winds. However, it must be emphasized that this comparison is based on the 3-second gust wind speed at 10 m height, and it should not be used as a comparison of the wind load effects on structures since the wind speed profiles for tornadic and synoptic winds differ. In other words, further inference with regard to structural reliability under tornado and synoptic wind loads should not be made based on this comparison alone. Similar analysis is carried out for the grid point located at 43.2165°N and 81.8670°W, which approximately represents the location of London Airport. The obtained results are shown in Figure 2.9b. The results show that the return period values of the maximum tornado wind speed are 208 (km/h) for T equal to 10^5 years, and 352 (km/h) for T equal to 10^6 years.

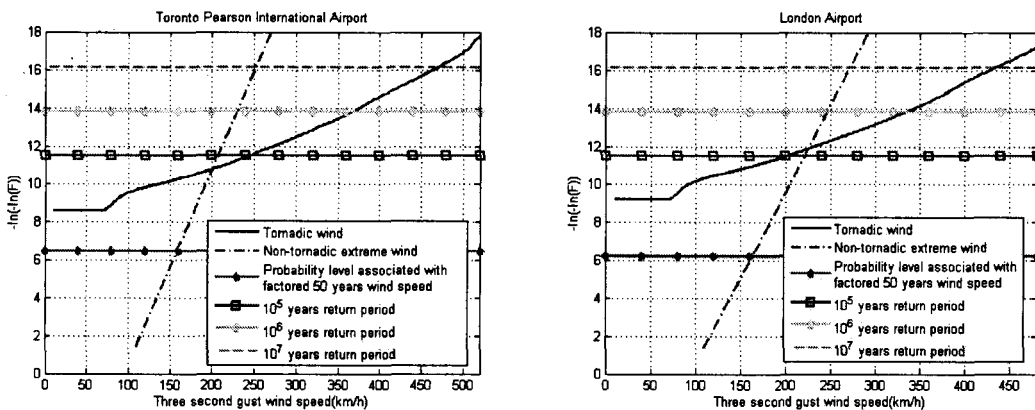


Figure 2.9 Probability distribution function of maximum tornado wind speed (3-second gust wind speed): a) for Toronto Pearson International Airport, b) for London Airport.

Note that in general the factored design wind speed for southern Ontario sites corresponds to a return period within 289 to 1938 years (Banik et al. 2007). The return period value of the maximum tornado wind speed for such a range of return periods is negligible. However, for some special structures such as nuclear power plants where extreme events with an annual probability of exceedance level as low as 10^{-7} are considered, the corresponding return period values of the maximum tornado wind speed are about 472 (km/h) for the location at 43.3931°N and 79.3590°W (Toronto), and 454 (km/h) at 43.2165°N and 81.8670°W (London).

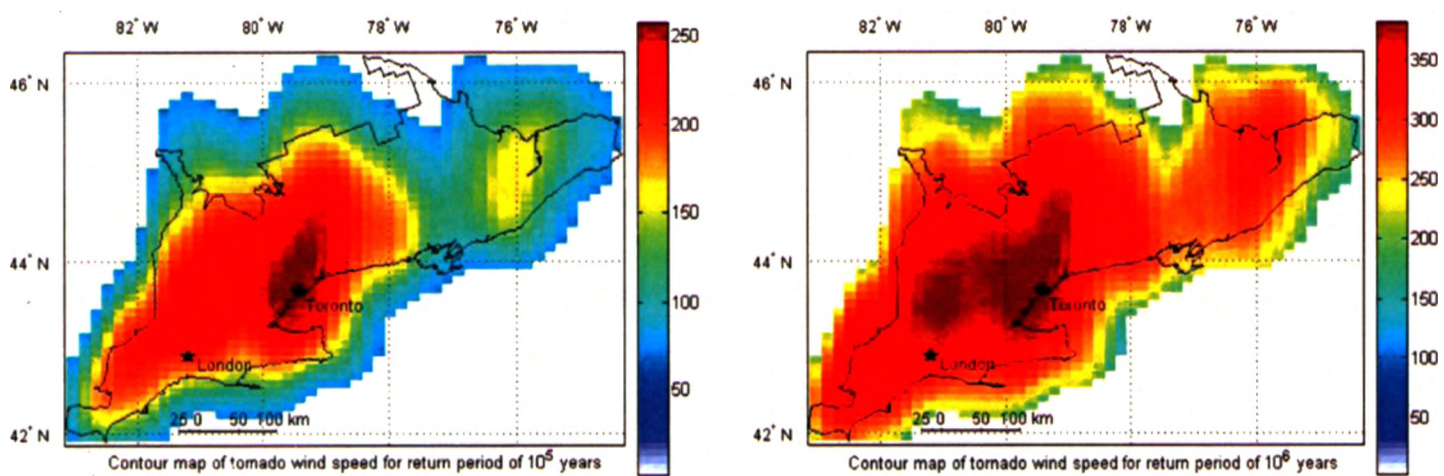


Figure 2.10 Contour map of tornado wind speed (3-second gust wind speed): a) for return period of 10^5 years, b) for return period of 10^6 years.

By repeating the above analysis, return period values for all the considered grid points can be obtained and used to construct the tornado hazard contour map for specified return period T . Alternatively, exceedance probabilities for a specified gust wind speed can be estimated at all considered grid points. These probabilities can be used to construct the contour map of exceedance probabilities. For example, by considering T equal to 10^5 and 10^6 years, return period values of the maximum tornado wind speed are calculated and shown in Figures 2.10a and 2.10b, respectively. The return period values shown in the

figures vary significantly from location to location.

To assess the differences between the return period values obtained by considering and ignoring the spatial inhomogeneous tornado occurrence, a tornado hazard analysis by assuming spatial homogeneous tornado occurrence is carried out, which leads to the return period values equal to 163 (km/h) for T equal to 10^5 years and about 323 (km/h) for T equal to 10^6 years. This 10^6 -year return period value agrees with that reported by Banik et al. (2008), while the value for T equal to 10^5 is somewhat different from that reported by Banik et al. (2007). The difference can be explained by noting that the latter uses Eqs. (2.3a) and (2.4) while this study is based on Eq. (2.3b). Comparison of these return period values to those shown in Figure 2.10 indicates that by ignoring the spatial inhomogeneity of tornado occurrence, significant overestimating of the tornado hazard results for the majority of the locations, while underestimation can be observed only for some area north of Toronto and London.

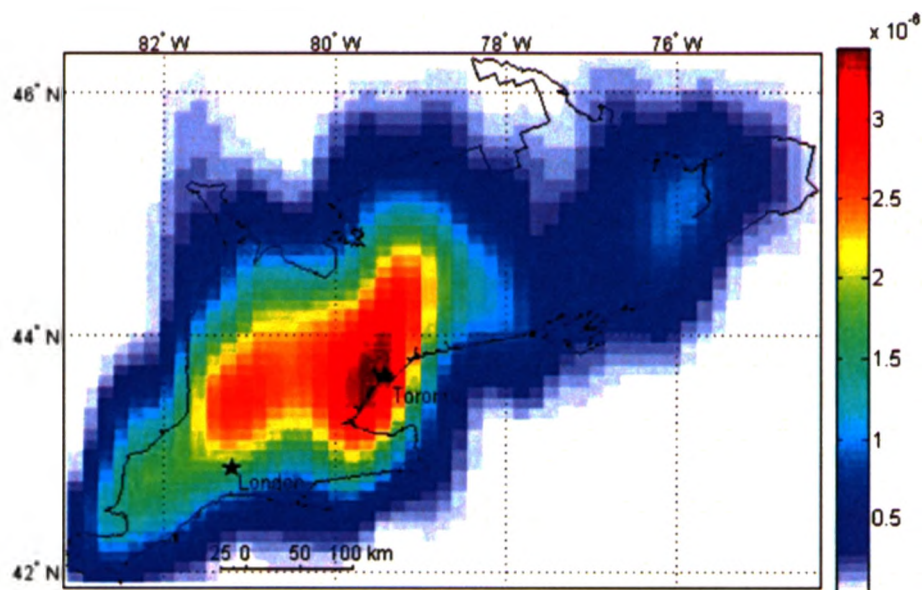


Figure 2.11. Contour map of exceedance probabilities for the maximum tornado wind speed (3-second gust wind speed) equal to 323 (km/h).

If a maximum wind speed of interest equal to 323 (km/h) is considered, the contour

map of exceedance probabilities is presented in Figure 2.11. The figure indicates that the exceedance probability level for the considered wind speed is higher than 10^{-6} for regions near Toronto and north of London. This observation is consistent with that can be drawn from Figure 2.10.

2.4 Conclusions

An assessment of the tornado hazard map considering the inhomogeneity of spatial tornado occurrence was carried out. The assessment adopts an existing probabilistic tornado wind field model, uses a spatial smoothing technique in evaluating the spatial tornado occurrence intensity, and employs simulation technique in assessing the probability distribution function of the tornado wind speed at grid points covering southern Ontario. The results presented in this chapter are used, for the first time, to provide quantitative tornado hazard maps for southern Ontario.

The analysis results indicate that the tornado striking rate for grid points of interest can be approximated very crudely by scaling the tornado occurrence intensity, since the ratios of the tornado striking rate to the tornado occurrence intensity vary somewhat for the considered region.

The obtained tornado hazard indicates that the return period value of the maximum tornado wind speed for return period corresponding to the factored design wind load is negligible. In other words, the tornado hazard at the factored design wind speed level is much smaller than the wind hazard due to synoptic winds even the spatial inhomogeneity of tornado occurrence is considered. Furthermore, the results show that the spatial inhomogeneity of the tornado occurrence has significant impact on the spatial tornado hazard level, and that return period values of tornado wind speed vary significantly over

the considered region. By ignoring the spatial inhomogeneity of tornado occurrence, the tornado hazard for areas north of City of Toronto and north of City of London is significantly underestimated while for other areas within the considered region, the tornado hazard is overestimated.

References

1. AIR. 2008. The Atlanta tornado. AIR Currents. Online publication by Applied Insurance Research, Boston, MA.
2. Banik, S.S., Hong, H.P. and Kopp, G.A. 2007. Tornado hazard assessment for southern Ontario. Canadian Journal of Civil Engineering, vol. 34, pp. 830-842.
3. Banik, S.S., Hong, H.P. and Kopp, G.A. 2008. Assessment of tornado hazard for spatially distributed systems in southern Ontario. Journal of Wind Engineering and Industrial Aerodynamics, vol. 96, pp. 1376-1389.
4. Bailey, T.C. and Gatrell, A.C. 1995. Interactive spatial data analysis. Longman Scientific and technical, London.
5. Dunn, W.L. and Twisdale, L.A. 1979. A synthesized windfield model for tornado missile transport. Journal of Nuclear Engineering and Design, vol. 52, pp. 135-144.
6. Durst, C.S. 1960. Wind speeds over short periods of time. Meteorological Magazine, vol. 89, pp. 181-186.
7. Etkin, D.A. 1999. Extreme events and natural disasters in an era of increasing environmental change. Report of Workshop on Emerging Environmental Issues in Ontario Environmental Monograph No.15. Institute for Environmental Studies, University of Toronto, pp. 19-22.
8. Fujita, T.T. and Pearson, A. 1973. Experimental classification of tornadoes in FPP scale. SMRP research paper no. 98, University of Chicago.
9. Garson, R.C., Morla-Catalan, J. and Cornell, C.A. 1975. Tornado risk evaluation using wind speed profiles. ASCE Journal of the Structural division, vol. 101, pp.

1167-1171.

10. Hangan, H. and Kim, J. 2006. Numerical simulations of tornado vortices. *Journal of Wind Engineering*, vol. 108, pp. 481-484.
11. Hoecker, W.H. 1960. Wind speed and air flow patterns in the Dallas tornado of 2 April 1957. *Monthly Weather Review*, vol. 88, pp. 167-180.
12. Hoecker, W.H. 1961. Three-dimensional pressure pattern of the Dallas tornado and some resultant implications. *Monthly Weather Review*, vol. 89, pp. 533-542.
13. King, P.W.S., Leduc, M.J., Sills, D.M.L., Donaldson, N.R., Hudak, D.R., Joe, P. and Murphy, B.P. 2003. Lake breezes in southern Ontario and their relation to tornado climatology, *Weather and Forecast*, vol. 19, pp. 22-42.
14. Kuo, H.L. 1970. Axisymmetric flows in the boundary layer of maintained vortex. *Journal of Atmospheric Sciences*, vol. 30, pp. 20-41.
15. Lewellen, D.C. and Lewellen, W.S. 2007, Near-surface intensification of tornado vortices, *Journal of Atmospheric Science*, vol. 64, pp. 2176-2194.
16. McDonald, J.R., Mehta, K.C., Minor, J.E. and Beason, L. 1975. Development of a wind speed risk model for the Argonne National Laboratory site, Report prepared by Institute for Disaster Research, Texas Tech University, Lubbock, Texas, May.
17. NBCC 2005. National building code of Canada. Institute for Research in Construction, National Research Council of Canada, Ottawa, Ontario.
18. Newark, M.J. 1984. Canadian tornadoes, 1950 -1979, *Atmosphere-Ocean*, vol. 22, pp. 343-353.
19. Nolan, D.S. 2005. A new scaling for tornado-like vortices, *Journal of Atmospheric Science*, vol. 62, pp. 2639-2645.

20. Nolan, D.S. and Farrell, B.F. 1999. The structure and dynamics of tornado-like vortices, *Journal of Atmospheric Science*, vol. 56(7), pp. 2908-2936.
21. Sigal, M.B., Singhal, A., Pan, K., Seneviratna, P., and Zadeh, M.M. 2000. Simulation of the tornado hazards in the U.S., *Proceedings of the 2000 Winter Simulation Conference*, pp. 1227-1234.
22. Sills, D.M.L. 1998. Lake and land breezes in southwestern Ontario: Observations, analyses and numerical modelling, Ph.D. thesis, York University, 338 pp.
23. Sills, D.M.L., Scriver, S.J. and King, P.W.S. 2004. The tornadoes in Ontario project (TOP). Preprints, 22nd AMS Conference on Severe Local Storms, Hyannis, MA, American Meteorological Society, CD-ROM 7B.5.
24. Thom, H.C.S. 1963. Tornado probabilities. *Monthly Weather Review*, vol. 93, pp. 730-736
25. Twisdale, L.A. 1978. Tornado data characterization and wind speed risk. *ASCE Journal of Structural Engineering*, vol. 104, pp.1611- 1630.
26. Twisdale, L.A., Dunn, W.L., Horie, Y. and Davis, T.L. 1981. Tornado Missile Simulation and design methodology, Vol.2, Model verification and database updates, Report prepared by Research Triangle Institute, Research Triangle Park, North Carolina, August 1981.
27. Twisdale, L.A. and Dunn, W.L. 1983. Probabilistic analysis of tornado wind risks. *ASCE Journal of the Structural division*. vol. 109, pp. 468-488.
28. Ward, N.B. 1972. The exploration of certain features of tornado dynamics using a laboratory model. *Journal of Atmospheric Science*, vol. 29, pp. 1194-1204.
29. Wen, Y.K. and Chu, S.L. 1973. Tornado risks and design wind speed. *ASCE Journal*

of the Structural division, vol. 99, pp. 2409-2421.

30. Wen, Y.K. 1975. Dynamic tornado wind loads on tall buildings. ASCE Journal of the structural division, vol. 101, pp. 169-178.

31. Ying, S.J. and Chang, C.C. 1970. Exploratory model study of tornado like vortex dynamics. Journal of Atmospheric Sciences, vol. 27, pp. 3-14.

CHAPTER 3

APPLICATION OF HIERARCHICAL BAYESIAN MODEL FOR ASSESSING TORNADO OCCURRENCE INTENSITY AND TORNADO HAZARD MAPS FOR SOUTHERN ONTARIO

3.1 Introduction

Tornados cause casualties and property damages. Southern Ontario is one of the regions in Canada that experiences significant tornado activities. Tornados are one of the most destructive natural hazards in terms of property damage and fatalities in the province of Ontario, Canada. A systematic tornado hazard assessment for the region has been carried out recently by Banik et al. (2007, 2008). Their assessment considered that the probabilistic tornado wind field model developed by Twisdale et al. (1981) is applicable for such hazard assessment, and that the spatial inhomogeneity of tornado occurrence for the region can be ignored. For the assessment, they employed the historical tornado catalogue described by Sills et al. (2004), which was developed based on the tornado database or historical tornado catalogue for Canada that was established by Newark (1984). They showed that at annual exceedance probability levels about or lower than 10^{-5} , the tornado hazard is more significant than that due to synoptic winds.

Rather than considering that the tornado occurrence can be modeled as homogeneous in space, a more realistic approach is to consider that the tornado occurrence in space is inhomogeneous, since lake breeze boundary generated convection may be the dominant mechanism for storm formation and lead to a preferred southwest-to-northeast axis of tornadic activity (Sills 1998). The spatial inhomogeneity of tornado occurrence was also discussed by King et al. (2003) and Banik et al. (2007). The consideration of this

inhomogeneity in assessing the tornado hazard map was presented in Chapter 2. The results show that the tornado hazard is site dependent. The results could also be valuable in selecting location of critical civil infrastructure facilities.

For the evaluation of the spatial inhomogeneity of tornado occurrence, the quartic kernel estimation technique (Bailey and Gatrell 1995) was used (see Chapter 2). This spatial smoothing technique is relatively simple and leads to clear description of spatial tornado occurrence pattern. However, it does not provide any information or characterization of the uncertainty in the tornado occurrence rate. It is noted that use of advanced statistical tools such as the hierarchical Bayesian modeling technique has been proposed for estimating the uncertainty in tornado occurrence intensity (Berliner 1996; Wikle and Anderson 2003). Such an uncertainty assessment for southern Ontario has not been conducted, and the impact of this uncertainty in estimating the tornado hazard has not been explored.

The main objective of this chapter is to investigate the degree of uncertainty in the spatially varying tornado occurrence rate, and to assess the impact of such an uncertainty in the estimated tornado hazard. The chapter is focused on the feasibility of such an assessment rather than provide a definitive evaluation of the uncertainty in the occurrence rate, and it is also focused on the crude sensitivity analysis of the tornado hazard to such an uncertainty. It must be emphasized that the assembled approach is aimed at providing a basis for more detailed and extensive analysis leading to a definitive tornado hazard map in the future. Therefore, the tornado hazard map provided in the present chapter should not be used as a definitive recommendation for the tornado hazard maps.

Steps leading to the assessed tornado hazard maps considering uncertainty in the

spatially varying tornado occurrence intensity are presented in the following.

3.2 Tornado catalogue and empirical spatial occurrence

A tornado database for Ontario was developed by Newark (1984) and subsequently updated by Sills et al. (2004). For each recorded historical tornado, the database contains some essential information such as tornado intensity in Fujita scale (*F*-scale), tornado occurrence time, geographic location of recorded tornado touchdown point, tornado direction of motion, and tornado length. Furthermore, the recorded tornado is identified as a confirmed, probable and possible tornado event. The confirmed category is defined so that events are considered as tornados due to visual evidence or damage reports. The probable category is used to describe events where all available evidence pointed to the likelihood of tornados, while the possible category is used to depict events whose associated evidence is either ambiguous or unreliable. Sills et al. (2004) recommended that one should use confirmed and probable events to represent the actual tornado touchdowns. This recommended criterion for selecting tornado events is adopted in the present chapter for events observed in southern Ontario between the year 1950 and 1992. These events are plotted in Figure 3.1. The considered time interval is chosen to be consistent with that of the tornado database of Ontario's neighbouring regions in the United States, since some of the probabilistic characteristics of tornado, which are not available from Ontario tornado catalogue, are available from the tornado database for the neighbouring regions (i.e., Michigan, Ohio, Pennsylvania and New York State), and could be considered for southern Ontario.

It has been argued that the reported tornado information in the tornado catalogue does not reflect the actual historical tornado activities due to reporting error and, bias and error

in tornado intensity classification. By considering both the de-trending (McDonald et al. 1975; Sigal et al. 2000) and error and bias correction (Twisdale et al. 1981), and by carrying out the analysis presented by Banik et al. (2007) for tornados observed in southern Ontario but with almost identical geographic regions, the obtained statistics for the tornados shown in Figure 3.1 are presented in Table 3.1.

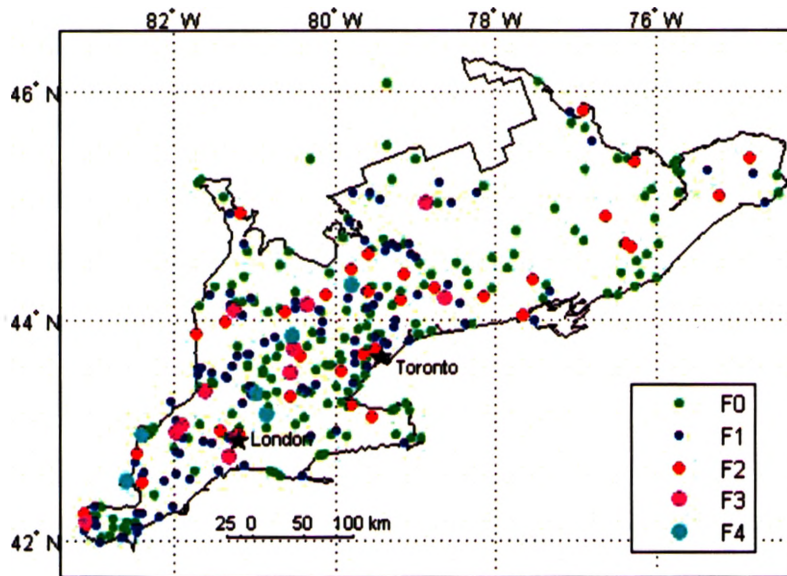


Figure 3.1. Confirmed and probable tornados for southern Ontario for the period 1950-1992

Table 3.1 Statistics of tornado occurrence for southern Ontario from 1950 to 1992.

F -scale	F -scale wind speed range (km/h)	N_o	N_c	$P''(F_j)$
F_0	64-116	196	280	0.4425
F_1	117-165	110	157	0.3101
F_2	166-216	37	37	0.1620
F_3	217-269	12	12	0.0567
F_4	270-335	6	6	0.0230
F_5	336-446	0	0	0.0057
Total		361	492	1

In the table, F_i , $i = 0, \dots, 5$, represents the classified tornado intensity (i.e., classified Fujita scale); the range of the updated wind speed for each tornado intensity category proposed by Twisdale et al. (1981); N_o represents the observed number of tornados; N_c represents the corrected number of tornados; and $P''(F_j)$ ($j = 0, \dots, 5$) represents the updated relative frequencies of tornado intensities adjusted for F -scale classification error analysis (Twisdale et al. 1981). Note that the updated occurrence rate of tornado with intensity F_i for southern Ontario, Λ_i per year equals $(492/43) \times P''(F_i)$.

Figure 3.1 indicates that the tornado occurrence intensity is spatially inhomogeneous, which is in agreement with the observation given by Sills (1998), King et al. (2003) and Banik et al. (2007). To better appreciate this spatial inhomogeneity, the number of tornado touchdowns is grouped in arbitrarily selected regular grid cells as shown in Figures 3.2a and 3.2b.

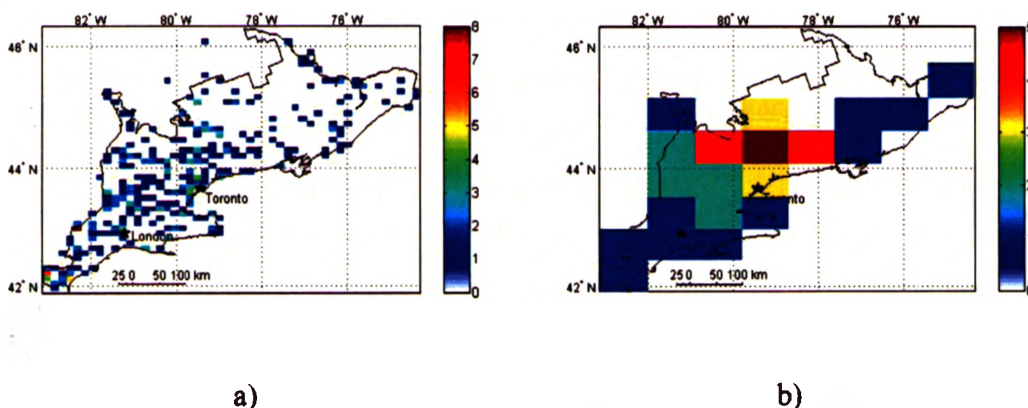


Figure 3.2. Tornado touchdown counts within selected regular grid cells based on tornado catalogue from 1950 to 1992: a) all tornados from 1950 to 1992 considering small grid cells; b) all tornados from 1985 to 1992 using large grid cells.

For the plot presented in Figure 3.2a, a regular 50×50 non-overlapping grid rectangular cells were employed to cover the considered region. In each cell, the total

number of tornado touchdown with intensity F_0 to F_5 from 1950 to 1992 is presented. It can be observed from the figure that the number of events in the cells varies, and there are many cells with zero counts. Furthermore, an assessment of tornado occurrence intensity by using two-dimensional quartic kernel estimation technique (Bailey and Gatrell 1995) could be used to define and confirm the spatial inhomogeneity of tornado occurrence intensity as shown in Chapter 2.

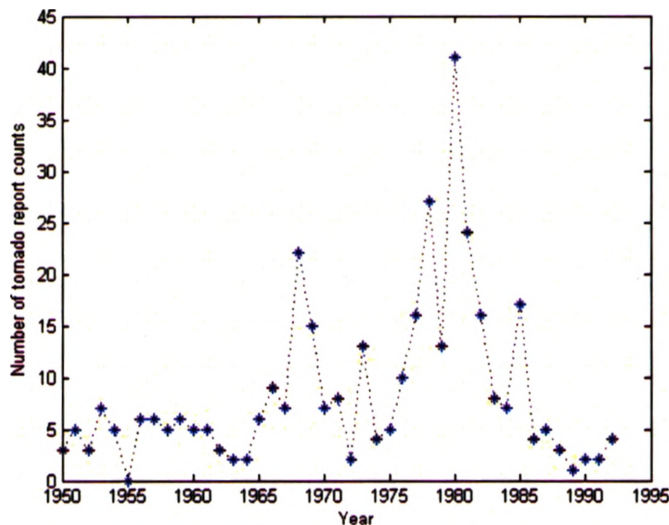


Figure 3.3 Time series of all tornado reports in southern Ontario from 1950 to 1992.

To illustrate the variability of tornado occurrence in time, the number of tornado events occurred in the considered geographic area from 1950 to 1992 is depicted in Figure 3.3. The figure seems to suggest that there appears to have an increased tornado occurrence activity for the considered region from 1950 to 1992. This increase may be due to the increase in population and improvement in detecting tornadoes (Marzban and Schaefer, 2001). To avoid possible errors caused by misreporting in tornado activities, an arbitrarily selected short tornado catalogue, say from 1985 to 1992, is considered. This consideration is justified since the short tornado catalogue is used only to illustrate the

applicability of assembled overall approach for assessing the tornado hazard that incorporates the uncertainty in the tornado occurrence intensity. Furthermore, use of a short tornado catalogue will significantly reduce the computing time for assessing the posterior probability distribution of the tornado occurrence intensity through the application of the hierarchical Bayesian model (Wikle and Anderson 2003), which will be discussed in the next section.

Since the considered number of the tornado events is very limited, a system with large cells as shown in Figure 3.2b is considered. In other words, a rectangular region covering southern Ontario is discretized into 64 cells, each with area of 5338 km², and the lowest left corner cell is centered at 41.908°N, and 83.121°W. For each cell, one could construct a time series of 8 years of number of annual tornado occurrence. Note that there are regions with no observations (e.g., water surface), and that tornados occurred in the neighbouring state in the USA are not considered. Figure 3.2b shows that there are many cells with zero number of tornado occurrence.

Comparison of the results shown in Figures 3.2a and 3.2b shows that use of a large and coarse grid cell system in general leads to smoother spatial distribution of tornado occurrence intensity. In other words, the selected grid cell system is likely to influence the estimated posterior probability distribution of the tornado occurrence intensity.

3.3 Bayesian estimate of tornado occurrence intensity

3.3.1 Hierarchical Bayesian model

An assessment of the uncertainty in tornado occurrence intensity and its impact on the tornado hazard for southern Ontario is not available in the literature. Such an assessment could be important if the estimated tornado hazard is significantly affected by such an

uncertainty. To appraise the importance of considering this uncertainty in evaluating tornado hazard, and to assess the complicated spatio-temporal dependence of tornado occurrence process, we adopt the hierarchical Bayesian model (Wikle and Anderson 2003) which is summarized in the following. The model is used to assess the posterior probability distribution of the tornado occurrence intensity. It basically updates the stochastic tornado occurrence process based on historical tornado catalogue through a series of conditional probabilistic models. In other words, the model decomposes the observed data into a series of conditional probabilistic models, and links all these probabilistic models together formally through basic probability relationships. The model incorporates three primary model representation stages: (1) data model represented by [data|process, parameters]; (2) process model represented by [process|parameters]; and (3) parameter model represented by [parameters], where the brackets refer to the “probability distribution” and the vertical line separates the uncertain variable(s) and condition(s). The relation between these models for updating tornado occurrence model can be formally expressed as:

$$\begin{aligned}
 & [\text{process}; \text{parameters} | \text{data}] \propto \\
 & [\text{data} | \text{process}; \text{parameters}] [\text{process} | \text{parameters}] [\text{parameters}] \quad (3.1)
 \end{aligned}$$

where the symbol \propto is used to denote the proportionality.

Since the tornado occurrence in space may be considered to be inhomogeneous, the expected number of events could be approximated by a generalized linear expression including spatial random effects. Furthermore, since historical tornado events may not necessarily occur at all considered cells, a zero-inflated Poisson model (Lambert 1992) can be used. Let $Y(s_i; t)$ denote the observed tornado counts in the i -th grid cell and at

time index t (representing the t -th year of interest). With a probability $p(s_i; t)$, this spatio-temporal process $Y(s_i; t)$ follows a Poisson process of mean occurrence intensity $\lambda(s_i; t)$. Furthermore, it is considered that the zero-inflated Poisson probability process $p(s_i; t)$ can be modeled on the logit scale or a logit model (Lambert 1992), and that $\lambda(s_i; t)$ can be expressed as the sum of linear temporal trend, and spatio-temporal random effects. The mathematical formulation and probabilistic models for $Y(s_i; t)$, $p(s_i; t)$ and $\lambda(s_i; t)$ as well as the parameter models for $p(s_i; t)$ and $\lambda(s_i; t)$ processes are summarized in Table 3.2.

The probabilistic models defining the parameters listed in Table 3.2 are given in Table 3.3 (Wikle and Anderson 2003), where $N(\cdot)$, $IG(\cdot)$ and $U(\cdot)$ denote normal, inverse gamma (Gelman, 2006) and uniform probability distributions with probability density function $f_N(x)$, $f_{IG}(x)$ and $f_U(x)$, respectively. These probability density functions are expressed as:

$$f_N(x; \mu, \sigma) = \frac{1}{\sqrt{2\pi}\sigma} \exp\left(-\frac{1}{2} \frac{(x - \mu)^2}{\sigma^2}\right) \quad (3.2a)$$

$$f_{IG}(x; q, r) = \frac{r^q}{\Gamma(q)} x^{-q-1} \exp\left(-\frac{r}{x}\right), \quad x > 0 \quad (3.2b)$$

and

$$f_U(x; u_1, u_2) = \begin{cases} \frac{1}{u_2 - u_1}, & \text{for } u_1 \leq x \leq u_2 \\ 0, & \text{otherwise} \end{cases} \quad (3.2c)$$

where x denote the random variable of interest, and μ , σ , q , r , u_1 and u_2 denote the probability distribution parameters.

Note that the original formulation given by Wikle and Anderson (2003) considered the El Niño (or El Niño/ Southern Oscillation (ENSO)) and La Niña events (the former and the latter refer to a periodic warming and cooling of ocean surface temperatures in the central and east-central equatorial Pacific). However, since evidence of this oscillation affecting the tornado occurrence activity in southern Ontario is very limited (Etkin et al. 2001), and a short tornado catalogue is used, the ENSO phenomenon is ignored in the present chapter for estimating the tornado occurrence intensity.

Based on the above considerations, given historical tornado catalogue (i.e., tornado counts), the posterior distribution of all processes and parameters, i.e. Equation (3.1), becomes:

$$\begin{aligned}
& [\lambda_1, \dots, \lambda_T, p_1, \dots, p_T, \alpha, \xi_1, \dots, \xi_T, \nu, a_1, a_2, \sigma_\varepsilon^2, \sigma_\xi^2, \sigma_{\delta,1}^2, \sigma_{\delta,2}^2, \sigma_\gamma^2, \sigma_\nu^2, \sigma^2, \theta, \theta_\xi | Y] \\
& \propto \left\{ \prod_{t=1}^T \prod_{i=1}^n [Y_i(s_i) \lambda(s_i; t), p(s_i; t)] [\lambda(s_i; t) | \alpha, \xi_t, \sigma_\varepsilon^2] [p(s_i; t) | \nu(s_i), \sigma_\gamma^2] \right\} \\
& \times \left\{ \prod_{t=1}^T [\xi_t | \delta, \theta_\xi, \sigma_\xi^2] [\sigma_\xi^2 | \theta_\xi] [\delta | \sigma_{\delta,1}^2, \sigma_{\delta,2}^2] [\sigma_{\delta,1}^2 | \sigma_{\delta,2}^2] [\nu | a_1, a_2, \sigma_\nu^2] [a_1 | a_2] [\sigma_\nu^2] \right. \\
& \left. \times [\alpha | \theta, \sigma^2] [\theta | \sigma^2] [\sigma_\varepsilon^2] \right\} \tag{3.3}
\end{aligned}$$

where Y denotes the tornado report counts, and λ , and p , are $n \times 1$ vectors of the n spatial locations at time t for the Poisson mean and non-zero-inflated probabilities respectively. The constant of proportionality equals the inverse of the multidimensional integration of the quantity shown on the right side of Eq. (3.1).

This constant of proportionality for the posterior probability distribution of all model processes and parameters (i.e., left side of Eq. (3.3)) is difficult, if not impossible, to obtain analytically, and use of numerical integration methods for its evaluation can be

Table 3.2 Summary of the adopted hierarchical Bayesian model (Wikle and Anderson 2003).

Process	Model formulation	Notes
$Y(s_i; t)$	$Y(s_i; t) \lambda(s_i; t), p(s_i; t)$ $\sim \begin{cases} \text{Pois}(\lambda(s_i; t)), & \text{with prob. } p(s_i; t); \\ 0, & \text{with prob. } 1 - p(s_i; t). \end{cases}$	“~” relates the stochastic process or random variable to its probabilistic model; $\text{Pois}(\lambda(s_i; t))$ denotes Poisson distribution with occurrence rate $\lambda(s_i; t)$; $1 - p(s_i; t)$ denotes the probability of zero-inflation.
$\lambda(s_i; t)$	$\log(\lambda(s_i; t))$ $= \beta(s_i)x_t + \eta(s_i; t) + \varepsilon(s_i; t)$ or $\log(\lambda(s_i; t)) = \Phi\alpha x_t + \Phi\xi_t + \varepsilon_t$	$\beta(s_i)$ represents the temporal trend is the regression parameter in grid cell s_i . $x_t = \{1, \dots, T\}$ is a year index, and the element of its correlation matrix is assumed to follow exponential model ($\exp(-\theta d)$, where d is the distance between cells); $\eta_t = (\eta(s_1; t), \dots, \eta(s_n; t))'$ represents the error process are spatially correlated and temporally uncorrelated; β and η_t are substituted by $\Phi\alpha$ and $\Phi\xi_t$, where Φ is an $n \times n$ matrix of Fourier basis functions; $\varepsilon(s_i; t) \sim iid N(0, \sigma_\varepsilon^2)$ represents the random effects that are not spatially correlated.
	$\alpha \theta, \sigma^2 \sim N(0, \sigma^2 \Sigma_\alpha(\theta))$	α is n dimensional vector; σ^2 is the variance of α ; the spatial correlation matrix of α , $\Sigma_\alpha(\theta)$, is assumed to be diagonal, with the diagonal elements corresponding to the spectral density depending on θ for the exponential correlation function. (see Yaglom, 1987, Shumway et al. 2000).
	$\xi_t \delta, \theta_\xi, \sigma_\xi^2 \sim N(\delta, \sigma_\xi^2 \Sigma_\xi(\theta_\xi))$, for all t ,	The mean of ξ_t , δ , has a normal prior $\delta \sigma_{\delta,1}^2, \sigma_{\delta,2}^2 \sim N(0, \text{diag}[\sigma_{\delta,1}^2, \sigma_{\delta,2}^2 1'_{n-1}])$ (diag[] denotes a diagonal matrix, $1'_{n-1}$ is a $1 \times (n-1)$ vector of ones); σ_ξ^2 is the variance of ξ_t ; similar with $\Sigma_\alpha(\theta)$, the spatial correlation matrix of ξ_t , $\Sigma_\xi(\theta_\xi)$, is assumed to be diagonal, with the diagonal elements corresponding to the spectral density depending on θ_ξ for the exponential correlation function.
$p(s_i; t)$	$\text{logit}(p(s_i; t)) = \nu(s_i) + \gamma(s_i; t)$	$\text{logit}(x) = \log(x/(1-x))$ is the logit function; $\nu(s_i)$ is a spatial random effect; $\gamma(s_i; t) \sim iid N(0, \sigma_\gamma^2)$ is an uncorrelated spatio-temporal error process.
	$\nu(s_i) a_1, a_2, \sigma_\nu^2$ $\sim N(a_1 z_1(s_i) + a_2 z_2(s_i), \sigma_\nu^2)$	$\nu(s_i)$ are independently for all i ; $z_1(s_i)$ and $z_2(s_i)$ are dummy variables indicating whether the grid-cell s_i is located “data rich” and “data poor” regions.

Table 3.3 Summary of the assigned priors and estimated posteriors for the model parameters and hyperparameters.

Parameter	Prior Mean	Prior Variance	Prior Hyperparameters	Posterior Mean	Posterior Variance
$\sigma_\epsilon^2 \sim IG(q_\epsilon, r_\epsilon)$	0.1	10	$q_\epsilon = 2.001, r_\epsilon = 0.1$	0.021	6.9×10^{-5}
$\sigma_\xi^2 \sim IG(q_\xi, r_\xi)$	0.5	10	$q_\xi = 2.025, r_\xi = 0.5$	0.029	2.7×10^{-4}
$\sigma^2 \sim IG(q, r)$	0.05	10	$q = 2, r = 0.05$	0.011	3.3×10^{-5}
$\theta \sim U(u_1, u_2)$	12.55	51.67	$u_1 = 0.1, u_2 = 25$	0.116	3.25×10^{-4}
$\theta_\xi \sim U(u_1, u_2)$	12.55	51.67	$u_1 = 0.1, u_2 = 25$	0.832	11.2
$\sigma_{\delta,1}^2 \sim IG(q_{\delta,1}, r_{\delta,1})$	30	100	$q_{\delta,1} = 11, r_{\delta,1} = 303$	28.9	86.8
$\sigma_{\delta,2}^2 \sim IG(q_{\delta,2}, r_{\delta,2})$	0.005	1	$q_{\delta,2} = 2, r_{\delta,2} = 0.005$	4×10^{-4}	1.6×10^{-8}
$\sigma_\gamma^2 \sim IG(q_\gamma, r_\gamma)$	0.2	2	$q_\gamma = 2.02, r_\gamma = 0.2$	0.163	1.96×10^{-2}
$\sigma_v^2 \sim IG(q_v, r_v)$	0.05	1	$q_v = 2.003, r_v = 0.05$	0.093	1.03×10^{-2}
$a_1 \sim N(\tilde{a}_1, \tilde{\sigma}_a^2)$	-0.1	10	$\tilde{a}_1 = -0.1, \tilde{\sigma}_a^2 = 10$	-1.26	0.66
$a_2 \sim N(\tilde{a}_2, \tilde{\sigma}_a^2)$	0.01	10	$\tilde{a}_2 = 0.01, \tilde{\sigma}_a^2 = 10$	-5.63	0.427

computing time consuming. However, the Markov Chain Monte Carlo (MCMC) sampling approaches (Gilks et al. 1996) can be employed to overcome the latter for assessing the posterior probability distribution. In such a case, the MCMC approaches are used to obtain samples from posterior distributions indirectly. More specifically, the MCMC methods are based on that a Markov chain can be constructed such that its stationary distribution coincides with the joint posterior distribution of model parameters. The initial values are assigned to the model parameters, and the chain is simulated until it converges to the stationary distribution. Samples within the burn-in period are ignored and those from the chain at stationarity are used to estimate the posterior distribution of model parameters. For the presented study, use of the Gibbs sampler, as a special case of MCMC method, is considered (Gilks et al. 1996, Brooks 2000).

The Gibbs sampler is well-adapted for the Bayesian analysis of complex statistical models, especially when the joint distribution of model parameters is not known explicitly but the conditional distribution of each parameter is known. The idea behind the Gibbs sampler is the use of the full conditional probability distributions. To clarify the Gibbs sampler in the context of Eq. (3.3), we note that the joint probability distribution of the model parameters, except a constant of normalization, is given on the right hand side of Eq. (3.3) as product of the prior probability distributions of model parameters and the likelihood function, which incorporates the observed tornado counts.

For simplicity of explanation, let ψ_1, \dots, ψ_n denote the set of model parameters and processes such as those shown on the left hand side of Eq. (3.3). Furthermore, let $[\psi_j | \psi_1, \dots, \psi_{j-1}, \psi_{j+1}, \dots, \psi_n]$ denote the full conditional probability distribution of ψ_j , which can be obtained based on the right hand side of Eq. (3.3) by algebraic manipulations. To generate samples of ψ_1, \dots, ψ_n , assign a set of initial values of ψ_1, \dots, ψ_n , denoted as $\psi_1^0, \dots, \psi_n^0$. Using the initial values, samples of ψ_1, \dots, ψ_n are generated using the full conditional distributions according to the following equation,

$$\begin{aligned}
 \psi_1^{k+1} &\sim [\psi_1 | \psi_2^k, \dots, \psi_n^k] \\
 \psi_2^{k+1} &\sim [\psi_2 | \psi_1^{k+1}, \psi_3^k, \dots, \psi_n^k] \\
 &\vdots \\
 \psi_n^{k+1} &\sim [\psi_n | \psi_1^{k+1}, \dots, \psi_{n-1}^{k+1}]
 \end{aligned} \tag{3.4}$$

where $\psi_1^k, \dots, \psi_n^k$ denote the k -th sample of ψ_1, \dots, ψ_n . The samples ($k = 1, \dots, n$), except those considered as within the “burn-in” period, can be used to construct the empirical posterior probability distributions or statistics of the model parameters

ψ_1, \dots, ψ_n . Note that use of the Gibbs sampler is facilitated if the full conditional probability distribution of each model process or parameter can be obtained easily.

In the present chapter, WinBUGS software (<http://www.mrc-bsu.cam.ac.uk/bugs/welcome.shtml>) is used to implement Gibbs sampler process. WinBUGS provides a graphical user interface and on-line monitoring and convergence diagnostics for Gibbs sampler process. Furthermore, it does not require the representation of the full-conditional distributions for each model parameter.

Note that, as indicated in Table 3.2, the spectral representations of the spatial processes β and η , (i.e., $\beta(s_i) = \Phi\alpha$ and $\eta(s_i; t) = \Phi\xi_t$) by using a matrix of Fourier basis functions Φ is considered. This representation is aimed at reducing the computational effort resulting from the high dimensionality of these two spatial processes. Note that vectors α and ξ_t are the discrete Fourier Transform (DFT) (Cooley and Tukey, 1965; Brigham, 1988) of β and η_t .

3.3.2 Estimation of tornado occurrence intensity

To estimate the posterior probability distribution shown in Eq. (3.3), values of the hyperparameters shown in Table 3.3 need to be assigned. Wikle and Anderson (2003) indicated that the prior distributions of hyperparameters are vague and the posterior estimates are not significantly sensitive to the values of the hyperparameters. Consequently, the prior values of hyperparameters used by Wikle and Anderson (2003) are adopted in this present study and shown in Table 3.3. Furthermore, rather than using a very refined rectangular cell system with all available recorded tornado activities, a relatively coarse cell system with available recorded tornado activities from 1985 to 1992

(see Figure 3.2b) is employed. This is aimed at reducing computing time to a manageable magnitude, and most importantly illustrating the analysis framework as well as demonstrating the feasibility of incorporating the posterior distribution of tornado occurrence intensity to assess the tornado hazard maps.

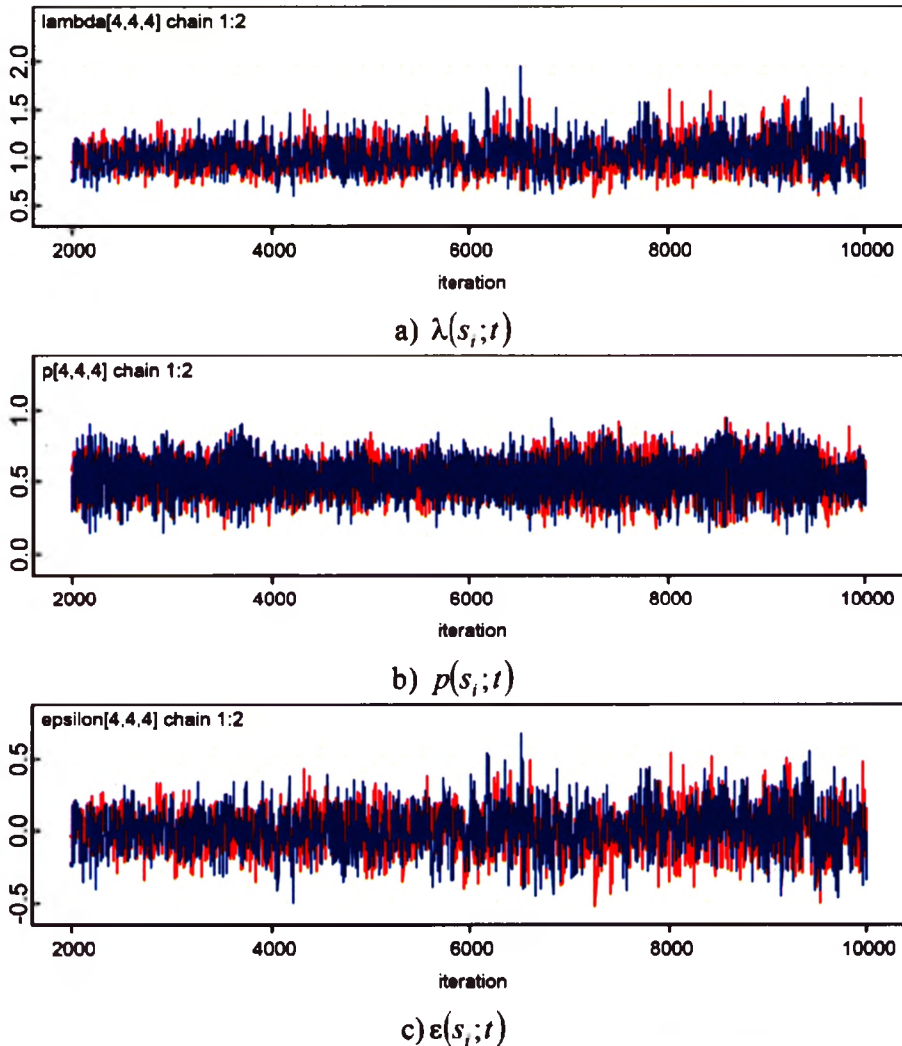
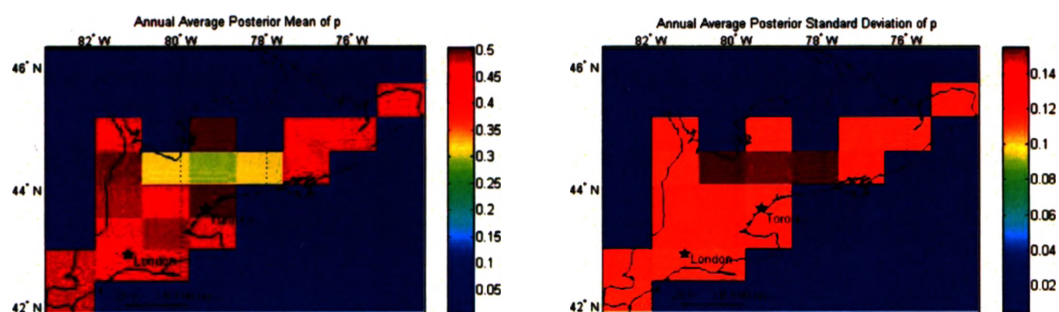


Figure 3.4 Illustration of samples of two chains considering $i=28$ and $t=4$ for: a) $\lambda(s_i; t)$, b) $p(s_i; t)$ and c) $\epsilon(s_i; t)$.

For the numerical analysis, simulation using the implemented MCMC method was carried out for 10,000 cycles and a “burn-in” period of 2000 cycles. The convergence of the simulation results was evaluated by comparing two simulated chains for the sampled

parameter values obtained by using two different set of initial values of the parameters, which can also be used to guide the selection of burn-in period. The sampled values of parameters $\lambda(s_i; t)$, $p(s_i; t)$ and $\varepsilon(s_i; t)$ for the cell representing the City of Toronto (i.e., $i = 28$) and for a particular time index t equal to 4 are shown in Figure 3.4 for two simulated chains. Visual inspection of the figure indicates that both sampled chains are stable. Test for assessing the accuracy of posterior estimates suggested by WinBUGS was carried out and test result was adequate.

The obtained posterior mean and variance of the model parameters are summarized in Table 3.3. Note that the counting process is completely characterized by two processes: the zero-inflation probability $p(s_i, t)$, and the occurrence rate of the Poisson process $\lambda(s_i, t)$. It is assumed that the logit of the zero-inflation probability is a function of $v(s_i)$ and $\gamma(s_i; t)$ (i.e., $\text{logit}(p(s_i; t)) = v(s_i) + \gamma(s_i; t)$). Table 3.3 shows that the mean of σ_v^2 is less than that of σ_γ^2 , indicating that the variability of $\text{logit}(p(s_i; t))$ (see Table 3.2) is likely to be more significantly affected by γ than by v . To inspect the spatial variability of $p(s_i; t)$, a plot of the obtained annual average posterior mean and standard deviation of $p(s_i; t)$ from 1985 to 1992 are shown in Figure 3.5. The figure indicates that the probability $p(s_i, t)$ is greater than 0.25 in the data-rich cells, while it can be significantly less than 0.05 for cells with scarce data. This is entirely consistent with the intention of using the zero-inflated Poisson model. Furthermore, the results indicate that there is significant uncertainty in the annual average $p(s_i, t)$. Note that the temporal variability of $p(s_i; t)$ for cells representing the City of Toronto and City of London are illustrated in Figure 3.6.



a) b)
 Figure 3.5 Annual average posterior mean and standard deviation of $p(s_i, t)$: a) Mean and b) Standard Deviation.

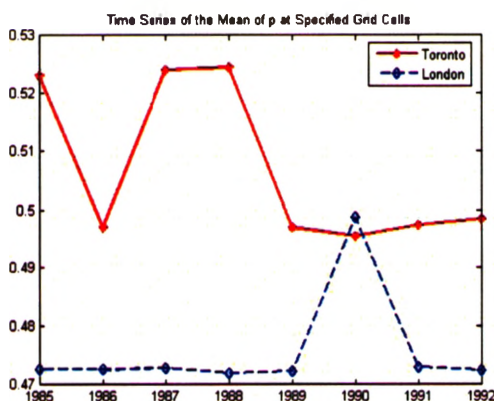


Figure 3.6 Time series of the mean of $p(s_i, t)$ for cells representing the City of Toronto and the City of London

The occurrence rate $\lambda(s_i, t)$ for the i -th cell was represented based on Fourier basis matrix Φ as shown in Table 3.2 (i.e., $\log(\lambda(s_i, t)) = \Phi\alpha x_i + \Phi\xi_i + \varepsilon_i$). Note that it is assumed that each element of the correlation matrix of β follows an exponential model with parameter θ (see Table 3.2) and, a small mean of θ leads to strong spatial dependence of $\beta(s_i)$ process. Therefore, since the posterior mean and standard deviation of θ shown in Table 3.3 are very small, it implies that $\beta(s_i)$ process is significantly spatially correlated.

The posterior mean and standard deviation of parameter $\beta(s_i)$ which is approximated by $\Phi\alpha$, are shown in Figure 3.7. The posterior mean of $\beta(s_i)$ presented in Figure 3.7a is clearly spatially varying. Relatively large positive values of $\beta(s_i)$ was found in the north region of southern Ontario indicating a positive temporal trend, whereas in most regions of south Ontario, especially for southwest Ontario including the City of Windsor, $\beta(s_i)$ is less than zero indicating a negative temporal trend. Furthermore, comparison with the total tornado reports shown in Figure 3.3, indicates that the large standard deviations are associated with data-sparse regions, which is expect.

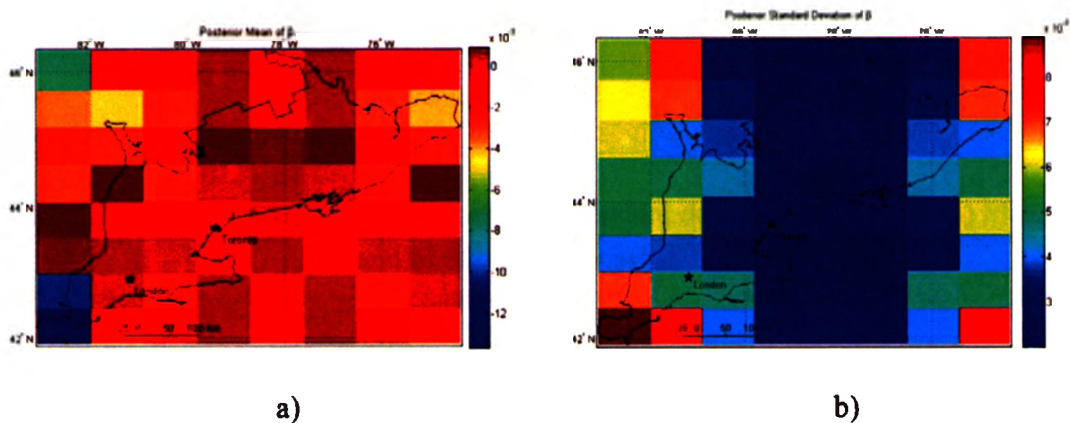


Figure 3.7 Posterior mean and standard deviation of $\beta(s_i)$: a) Mean, and b) Standard deviation.

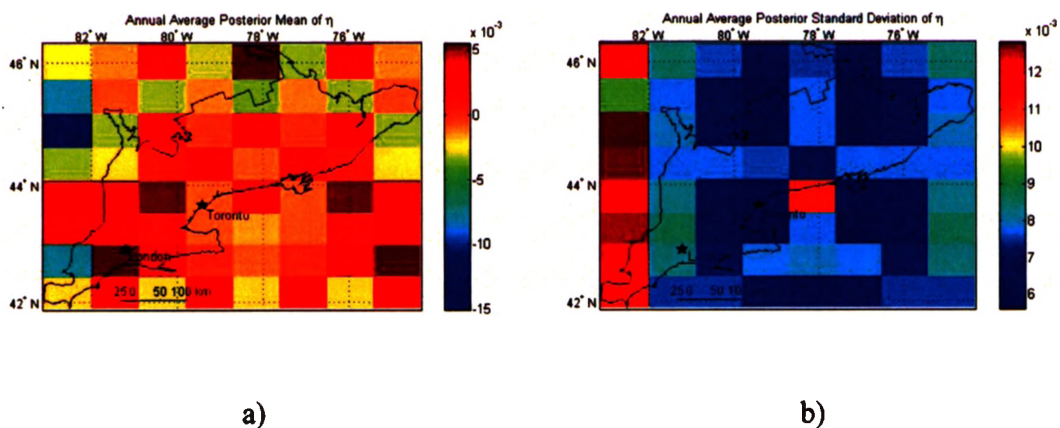


Figure 3.8 Annual average posterior mean and standard Deviation of $\eta(s_i; t)$: a) Mean, and b) Standard deviation.

The process $\eta(s_i; t)$ is not spatially significantly correlated since the parameter characterizing the spatial correlation of ξ_t , θ_ξ , is associated with a significant mean and standard deviation as shown in Table 3.3. The posterior mean and standard deviation of η_t are shown in Figure 3.8.

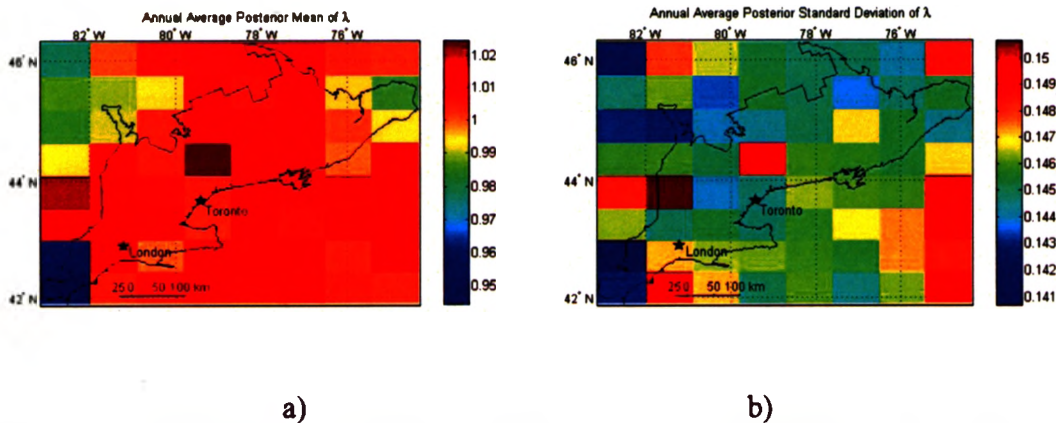


Figure 3.9 Annual average posterior mean and standard deviation of $\lambda(s_i; t)$: a) Mean and b) Standard deviation.

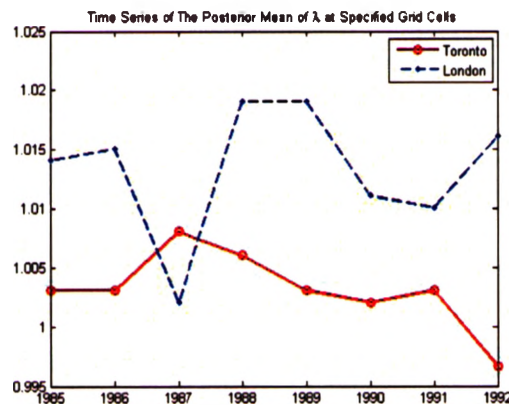


Figure 3.10 Time series of the mean of $\lambda(s_i; t)$ at specified grid cells representing the city of Toronto and London

To inspect the variability of $\lambda(s_i; t)$, a plot of the obtained annual average posterior mean and standard deviation of $\lambda(s_i; t)$ from 1985 to 1992 are shown in Figure 3.9, while

the temporal variability of $\lambda(s_i; t)$ for grid cells representing the City of Toronto and the City of London is shown in Figure 3.10. These figures indicate that the rate of $\lambda(s_i; t)$ is spatio-temporally varying and with significant uncertainty.

3.4 Tornado hazard maps

3.4.1 Adopted formulation and probability distribution of tornado wind speed

The assessment of the tornado hazard in terms of wind speed requires the use of tornado wind field model and the tornado occurrence intensity for the sites of interest. The former can be used to establish the probability distribution of tornado wind speed, while the latter can be used to estimate the tornado striking rate. Both of these are needed for estimating the probability that the maximum wind speed due to tornado, V , exceeds a specified value v in a time period T (years) for a point of interest, $P_T(V > v)$, which can be expressed as,

$$P_T(V > v) \approx \sum_{i=0}^{n_{\max}} (1 - \exp(-\gamma_{Ai} P(V > v | F_{Ai}) T)) \quad (3.5)$$

where γ_{Ai} is the annual rate of tornado striking at the point of interest with striking intensity F_{Ai} , and $P(V > v | F_{Ai})$ denotes the probability that V is greater than v conditioned on the striking intensity F_{Ai} . In deriving the above equation, it is considered that the tornado striking a point can be modeled as Poisson process, the striking intensity of tornado F_{Ai} represents the “actual” tornado striking intensity rather than the tornado intensity according to its classification F_i (in F -scale, that is Fujita scale). The distinction between F_{Ai} and F_i is necessary since the latter contains tornado intensity that is less than

or equal to the classified intensity along the tornado path length (Twisdale et al. 1983). More detailed derivation leading to Eq. (3.5) can be found in Chapter 2.

By adopting the probabilistic tornado wind field model and statistics of the model parameters, the estimated probability distributions of tornado wind speed conditioned on the striking intensity F_{Ai} by using the simulation technique is depicted in Figure 3.11. These probability distributions are to be employed for assessing tornado hazard maps.

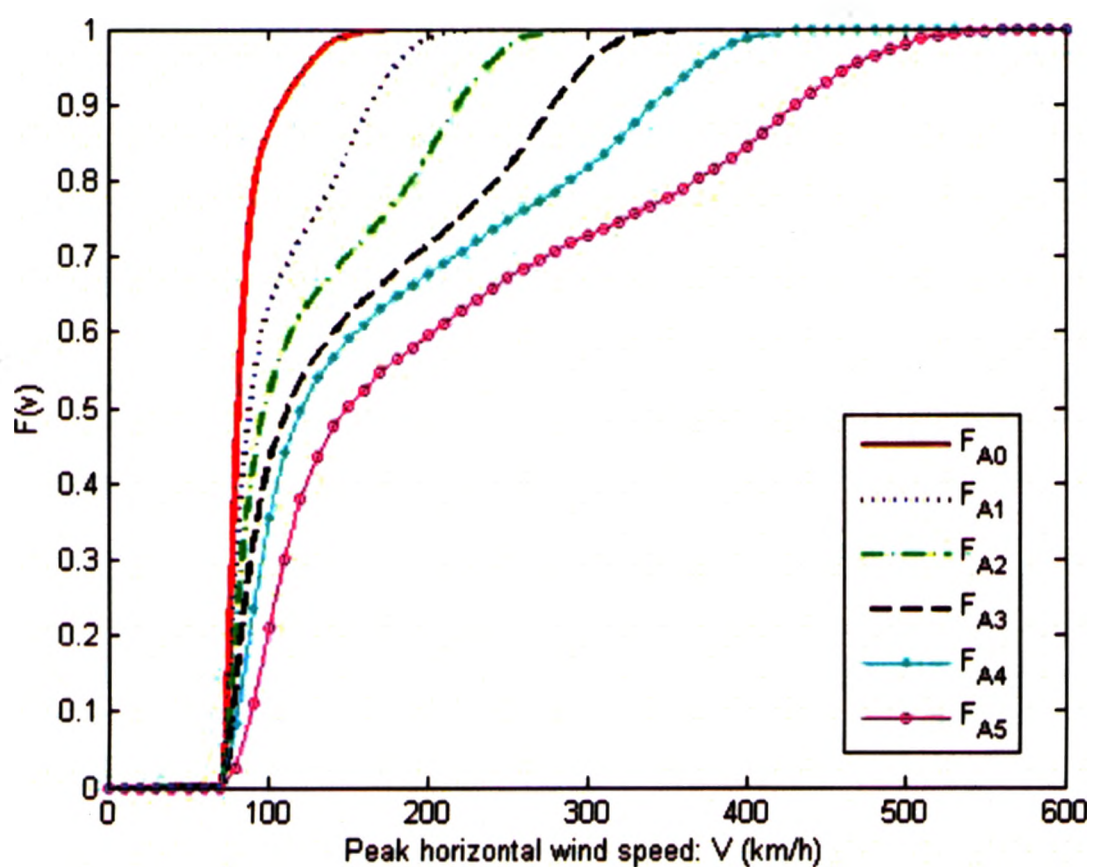


Figure 3.11 Probability distribution function of maximum tornado horizontal wind speed (3 second gust wind speed) for a randomly selected point within the striking area.

3.4.2 Estimated tornado contour maps

The estimation of tornado hazard by using Eq. (3.5) requires the annual tornado striking rate γ_{Ai} . This rate can be estimated based on the tornado occurrence model described in Section 3.4.1. Two cases will be considered. In Case 1, it is considered that the uncertainty in the occurrence rate $\lambda(s_i, t)$ and the zero-inflation probability $1-p(s_i, t)$ can

be ignored, and use of their posterior means in estimating the striking rate is sufficient adequate. In Case 2, it is considered that the occurrence rate $\lambda(s_i, t)$ equals the posterior mean plus one standard deviation, and $p(s_i, t)$ equals its posterior mean. It is expected that comparison of the results for Cases 1 and 2 can be used to illustrate the impact of the uncertainty in the occurrence rate on the estimated tornado hazard.

Other probabilistic models such as the probability distribution of (classified) tornado intensity, path length, path width, and path direction were already discussed in Chapter 2. These models are to be adopted in the present chapter.

Given the occurrence rate (i.e., Case 1 or Case 2) and probability of zero-inflation, one can estimate the rate of striking for sites of interest according to the following steps:

- 1) Sample tornado touchdown site (i.e., tornado origin) according to the (spatial) tornado occurrence intensity defined by $\lambda(s_i, t)$ and $p(s_i, t)$;
- 2) Sample the tornado intensity according to $P''(F_i)$ ($i = 0, \dots, 5$), the tornado path direction, path length and path width based on the probabilistic models described in the previous Chapter 2;
- 3) Sample the percentage of the path length whose striking intensity within the path length is F_{Aj} according to the tornado intensity variation along the tornado track length given by Twisdale et al. (1981);
- 4) Superimpose the tornado damage area on the region of interest and check whether a grid point is within the tornado damage area of intensity F_{Aj} ; and
- 5) Repeating 1) and 5) n_E times to estimate γ_{Aj} for all the considered grid points where n_E is the total number of tornado events occurred within Ω_S and time interval of interest.

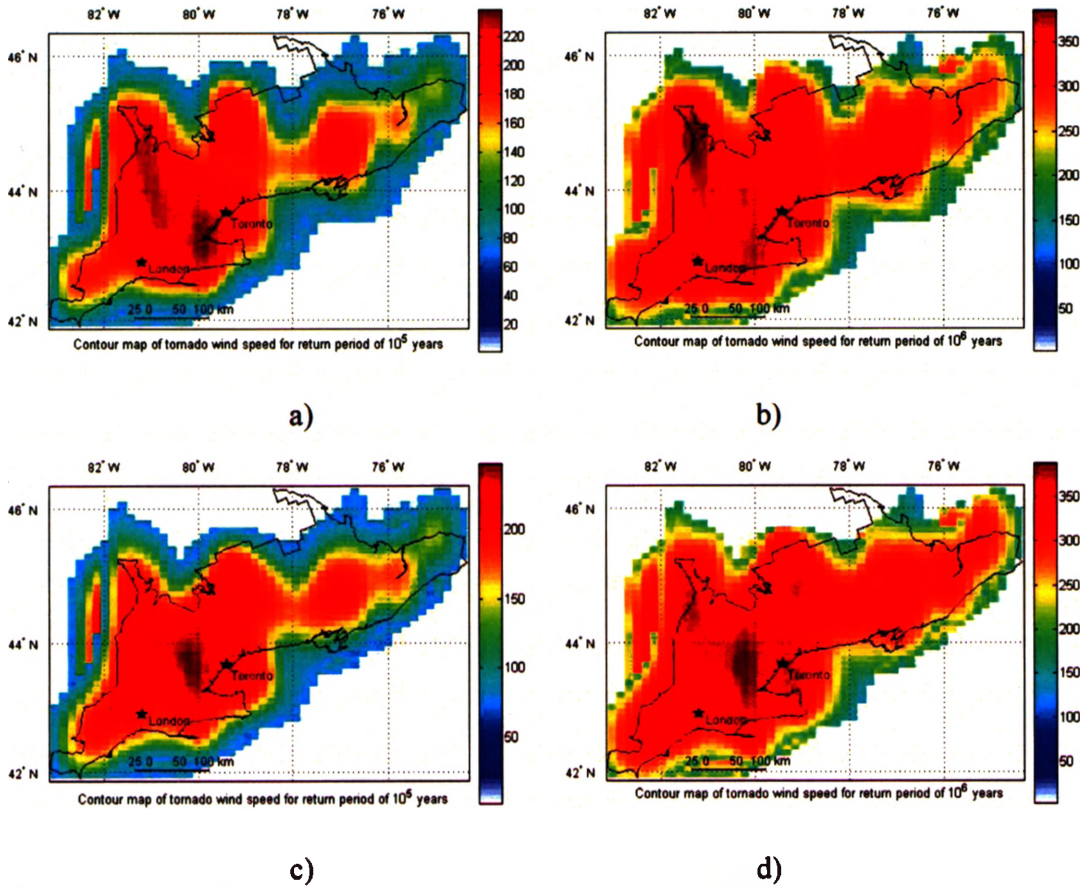


Figure 3.12 Contour map of return period values of tornado wind speed for Cases 1 and 2: a) Case 1 with return period equal to 10^5 , b) Case 1 with return period equal to 10^6 , c) Case 2 with return period equal to 10^5 , d) Case 2 with return period equal to 10^6 .

Using the estimated striking rate for each striking intensity F_{A_j} , the probability distribution of the tornado wind speed conditioned on the striking rate and Eq. (3.5), the tornado hazard in terms of the return period values is evaluated and shown in Figure 3.12 for selected (regular) grid points for both Case 1 and Case 2. Note that for Case 1, the 10^5 and 10^6 -year return period values of the tornado wind speed are, respectively, equal to 206 (km/h) and 350 (km/h) for the City of Toronto, and are equal to 202 (km/h) and 346 (km/h) for the City of London. This shows that the return period values for the former are greater than the latter, which is consistent with the findings in Chapter 2.

However, the differences are much smaller, which can be explained by noting that the results for Chapter 2 is based on tornado catalogue from 1950 to 1992, while those for the present chapter is based on tornado catalogue from 1985 to 1992. Furthermore, the cells employed for assessing the tornado occurrence rate are coarse and could lead to inaccurate representation of the tornado occurrence intensity.

The results for Case 2 indicate that the 10^5 and 10^6 -year return period values of tornado wind speeds are equal to 230 (km/h) and 366 (km/h) for the City of Toronto, and are equal to 204 (km/h) and 358 (km/h) for the city of London. Comparison of the results for Case 1 and Case 2 suggests that the uncertainty in tornado occurrence rate could affect the assessed tornado hazard. Therefore, this uncertainty as well as the size of the adopted cells need to be investigated further in a future study for assessing the tornado hazard contour maps by using all available tornado catalogue.

It must be emphasized again that the intention of this assessment is focused on the parametric study of the impact of the uncertainty in the tornado occurrence intensity on the estimated tornado hazard rather than providing a definitive recommendation for the tornado hazard maps.

3.5. Discussion and conclusions

The hierarchical Bayesian modeling technique has been adopted and successfully implemented to estimate the tornado occurrence intensity. The obtained probabilistic model of tornado occurrence rate is used in estimating the tornado striking rate which is needed in assessing tornado hazard and evaluate the tornado wind speed contour maps. Although the obtained results cannot be used to recommend definitive tornado hazard

maps, it showed that it is feasible in using such an assembled approach to assess the tornado hazard maps, which incorporating the uncertainty in tornado occurrences.

Conclusions based on the preliminary analysis results include:

- a) The estimated return period values of the tornado wind speed are sensitive to the considered tornado catalogue. Therefore, it is desirable to use a long tornado catalogue for such estimation.
- b) The size of the cells considered in estimating the posterior statistics of the tornado occurrence can affect the spatial distribution of tornado occurrence intensity, and careful consideration and further parametric study must be conducted in selecting the size of the cells.

References

1. Bailey, T.C. and Gatrell, A.C. 1995. *Interactive spatial data analysis*. Longman Scientific and technical, London.
2. Banik, S.S., Hong, H.P. and Kopp, G.A. 2007. Tornado hazard assessment for southern Ontario. *Canadian Journal of Civil Engineering*, vol. 34, pp. 830-842.
3. Banik, S.S., Hong, H.P. and Kopp, G.A. 2008. Assessment of tornado hazard for spatially distributed systems in southern Ontario. *Journal of Wind Engineering and Industrial Aerodynamics*, vol. 96, pp. 1376-1389.
4. Berliner, L.M. 1996. Hierarchical Bayesian time series models. In: *Maximum Entropy and Bayesian Methods*: Hanson, K. and Silver, R. (Eds.), , pp. 15-22.. Kluwer Academic Publishers, Dordrecht, Netherlands.
5. Brigham, E.O. 1988. *The fast Fourier transform and its applications*. Prentice Hall, Englewood Cliffs, New Jersey.
6. Brooks, H. E. 2000. Severe thunderstorm climatology: What we can know. Preprints, 20th Conference on Severe Local Storms, Orlando, Florida, American Meteorological Society, pp. 126-129.
7. Cooley, J.W. and Tukey, J.W. 1965. An algorithm for the machine calculation of complex Fourier series. *Mathematics of Computation*, vol. 19, pp. 297-301.
8. Etkin, D., Brun, S. E., Shabbar, A. and Joe, P. 2001. Tornado climatology of Canada revisited: Tornado activity during different phases of ENSO. *International Journal of Climatology*, vol. 21, pp. 915-938.
9. Gelman, A. 2006. Prior distributions for variance parameters in hierarchical models. *Bayesian Analysis*, vol. 1, pp. 515-533.

10. Gilks, W.R., Richardson, S., and Spiegelhalter, D.J. (Eds.) 1996. Markov Chain Monte Carlo in Practice. Chapman and Hall, London.
11. Lambert, D. 1992. Zero-inflated Poisson regression, with an application to defects in manufacturing. *Technometrics*, vol. 34, pp. 1-14.
12. Marzban, C. and Schaefer, J. T. 2001. The correlation between U. S. tornadoes and Pacific sea surface temperatures. *Monthly Weather Review*, vol. 129, pp. 884-895.
13. McDonald, J.R., Mehta, K.C., Minor, J.E. and Beason, L. 1975. Development of a wind speed risk model for the Argonne National Laboratory site, Report prepared by Institute for Disaster Research, Texas Tech University, Lubbock, Texas, May.
14. Newark, M.J. 1984. Canadian tornadoes, 1950 -1979. *Atmosphere-Ocean*.22, pp. 343-353.
15. King, P.W.S., Leduc, M.J., Sills, D.M.L., Donaldson, N.R., Hudak, D.R., Joe, P. and Murphy, B.P. 2003. Lake Breezes in Southern Ontario and Their Relation to Tornado Climatology, *Weather and Forecast*, vol. 19, pp.22-42.
16. Shumway, R.H. and Stoffer, D.S. 2000. *Time Series Analysis and its Applications*. Springer-Verlag, New York.
17. Sigal, M.B., Singhal, A., Pan, K., Seneviratna, P., and Zadeh, M.M. 2000. Simulation of the tornado hazards in the U.S., *Proceedings of the 2000 Winter Simulation Conference*, pp. 1227-1234.
18. Sills D. M. L. 1998. Lake and land breezes in southwestern Ontario: Observations, analyses and numerical modelling, Ph.D. thesis, York University, 338 pp.

19. Sills, D. M. L., Scriver, S. J. and King, P. W. S. 2004. The tornadoes in Ontario project (TOP). Preprints, 22nd AMS Conference on Severe Local Storms, Hyannis, MA, Amer. Meteorol. Soc., CD-ROM 7B.5.
20. Twisdale, L.A., Dunn, W.L., Horie, Y. and Davis, T.L. 1981. Tornado Missile Simulation and design methodology, Vol.2, Model verification and database updates, Report prepared by Research Triangle Institute, Research Triangle Park, North Carolina, August 1981.
21. Twisdale, L.A. and Dunn, W.L. 1983. Probabilistic analysis of tornado wind risks. ASCE Journal of the Structural division. vol. 109, pp 468-488.
22. Wikle, C.K. and Anderson, C.J. 2003. Climatological analysis of tornado report counts using a hierarchical Bayesian spatio-temporal model. Journal of Geophysical Research-Atmospheres, vol. 108, No. D24, 9005, doi: 10.1029/2002JD002806.
23. Wikle, C.K. and Hooten, M.B. 2005. Hierarchical Bayesian Spatio-Temporal Models for Population Spread. In: Applications of Computational Statistics in the Environmental Sciences: Hierarchical Bayes and MCMC Methods. Clark, J.S. and Gelfand, A. (Eds), Oxford University Press.
24. Yaglom, A.M. 1987. Correlation theory of stationary and related random functions. Vol. I: Basic Results. Springer-Verlag, New York.

CHAPTER 4

CONCLUSIONS AND RECOMMENDED FUTURE STUDIES

4.1 Conclusions

An assessment of the tornado hazard maps considering the inhomogeneity of spatial tornado occurrence was carried out. The results presented in this study are used, for the first time, to provide quantitative tornado hazard maps for southern Ontario. Although the maps (see Chapter 2) do not incorporate the uncertainty in spatial variability of tornado occurrence intensity, they can be used to aid the infrastructure planning activities.

The analysis results indicate that the tornado striking rate for grid points of interest can be approximated very crudely by scaling the tornado occurrence intensity, since the ratios of the tornado striking rate to the tornado occurrence intensity vary somewhat for the considered region. The obtained tornado hazard indicates that the tornado hazard at the factored design wind speed level is much smaller than the wind hazard due to synoptic winds even if the spatial inhomogeneity of tornado occurrence is considered. Furthermore, the results show that the spatial inhomogeneity of the tornado occurrence has significant impact on the spatial tornado hazard level, and that return period values of the tornado wind speed vary significantly over the considered region. By ignoring the spatial inhomogeneity of tornado occurrence, the tornado hazard for areas near the City of Toronto and north of City of London is significantly understimated while for other areas within the considered region, the hazard is overestimated. Therefore such inhomogeneity must be considered in developing any quantitative tornado hazard maps.

To incorporate the uncertainty in the tornado occurrence rate in time and space, the hierarchical Bayesian modeling technique has been adopted and successfully

implemented to estimate the tornado occurrence intensity as shown in Chapter 3. The obtained probabilistic model of tornado occurrence rate is used in estimating the tornado striking rate which is needed in assessing tornado hazard and evaluate the tornado wind speed contour maps. Although the obtained results cannot be used to recommend definitive tornado hazard maps, they showed that it is feasible to use such an assembled approach to assess the tornado hazard maps, which incorporating the uncertainty in tornado occurrences.

4.2 Recommended future studies

It is recommended that a further parametric study is to be carried out to investigate the impact of the uncertainty in the tornado occurrence on the estimated tornado hazard using the assemble approach shown in Chapter 3. In such an analysis, the uncertainty in temporal variability of tornado occurrence may be ignored due to insufficient statistical data. Also it is desirable to adopt or develop a probabilistic tornado wind field model, that is capable of describing the observed physical phenomena of the tornados, for tornado hazard assement.

Finally, since probabilistic quantitative tornado hazard maps for Canada are not available at present, and are valuable for emergency palnning and insurance industry, assessment of these maps needs to be carried out.

APPENDIX A

ADOPTED TORNADO WIND FIELD MODEL

The adopted wind field model for the present study is the one developed by Dunn and Twisdale (1979) and Twisdale et al. (1981, 1983). This wind field model, according to the authors, relies on probabilistic characteristics associated with description of the phenomena, and contains variable flow features. Tornado wind field includes equations that can be used to estimate tangential, vertical and radial wind speeds. An illustration of the predicted tornado wind field was already shown in Figure 3.3.

According to their model, the tornado translational wind speed, U_T , affects the wind velocity experienced by a structure that is located on the left or right side of the tornado vortex center, and leads to the tornado wind field that becomes asymmetric. The degree of asymmetry depends on the magnitude of U_T . It was suggested that for each given tornado intensity in F -scale U_T can be modeled as a truncated normal variate with probability density function $f_{U_T}(U_T)$ given by,

$$f_{U_T}(U_T) = \frac{\frac{1}{\sigma_{U_T}} \phi\left(\frac{x - \mu_{U_T}}{\sigma_{U_T}}\right)}{\Phi\left(\frac{U_{U_T} - \mu_{U_T}}{\sigma_{U_T}}\right) - \Phi\left(\frac{L_{U_T} - \mu_{U_T}}{\sigma_{U_T}}\right)}, \quad L_{U_T} < U_T < U_{U_T} \quad (\text{A.1})$$

where $\phi(\bullet)$ and $\Phi(\bullet)$ denote the standard normal probability density function and standard normal probability distribution function, respectively, the upper bound U_{U_T} and lower bound L_{U_T} are given in Table A.1, the $\mu_{U_T} = (U_{U_T} + L_{U_T})/2$, and the σ_{U_T} is considered to be proportional to $(U_{U_T} - L_{U_T})$.

To describe the tornado wind field model, there is a need to provide the ratio of the radial velocity U_r to tangential velocity U_θ , denoted by γ . This ratio is also known as radial inflow factor. An increasing in γ leads to an increased vertical velocity inside the vortex core, and a higher wind speed across the tornado width for the same reference maximum wind speed. It is suggested (Twisdale et al. 1981) that γ can be modeled as a truncated normal variable within 0.3 and 1.4, with mean equal to 0.7 and standard deviation (before truncation) equal to 0.2.

Table A.1 Tornado translation speed (fastest quarter mile gust winds) characterization

<i>F</i> -Scale Intensity	Truncated Normal Probability Distribution Parameters			
	Lower bound (L_{U_r}) (km/h)	Upper bound (U_{U_r}) (km/h)	Mean (μ_{U_r}) (km/h)	Std. Deviation (σ_{U_r}) (km/h)
F_0	8	56	32	12
F_1	8	72	40	15.36
F_2	8	80	48	16.64
F_3	8	88	56	17.6
F_4	8	104	72	20.16
$\geq F_5$	8	120	88	22.4

Other parameters need to be specified for the tornado wind field include the radius ρ_{m0} to the maximum tangential velocity at a specified height z_0 , and the boundary layer thickness $\delta(\rho)$, where ρ is the radial distance from the vortex center. ρ_{m0} affects the tornado wind field in many ways and it varies significantly (strictly speaking, ρ_{m0} varies during its life cycle). Based on the investigation of historical tornados, Twisdale et al. (1981) suggested again that ρ_{m0} can be modeled as a truncated normal variable with the parameters shown in Table A.2.

The reference elevation z_0 represents the average value of the height of structures and trees associated with the damage descriptions of the tornado intensity classification system, and can be taken to be equal to 10 m (i.e. 33 ft) above the ground surface.

Table A.2 Characteristics of tornado core radius.

F-Scale Intensity	Truncated Normal Probability Distribution Parameters			
	Lower bound of ρ_{m0} (m)	Upper bound of ρ_{m0} (m)	Mean $m_{\rho_{m0}}$ (m)	Standard deviation $\sigma_{\rho_{m0}}$ (m)
F_0, F_1	$\min(0.1 \times W, 30.48)$	$\min(0.2 \times W, 121.92)$	$\min(0.15 \times W, 76.2)$	$\min(0.025 \times W, 22.86)$
F_2, F_3	$\min(0.1 \times W, 60.96)$	$\min(0.2 \times W, 167.64)$	$\min(0.15 \times W, 114.3)$	$\min(0.025 \times W, 26.67)$
$\geq F_4$	$\min(0.1 \times W, 91.44)$	$\min(0.2 \times W, 213.36)$	$\min(0.15 \times W, 152.4)$	$\min(0.025 \times W, 30.48)$

The variable core radius ρ_m along the height where the tangential velocity is maximum depends on the boundary layer thickness, and is calculated using,

$$\rho_m = \begin{cases} \rho_{m0} + S(z - z_0), & z \leq \delta(\rho) \\ \rho_{m0} + S(\delta(\rho) - z_0), & z > \delta(\rho) \end{cases} \quad (\text{A.2})$$

where S is the core slope that is considered to be uniformly distributed between 0 to 0.3 and is considered to be applicable to all heights within the boundary layer. The thickness of the boundary layer thickness, $\delta(\rho)$, is a function of the radial coordinate ρ , and is given by,

$$\delta(\rho) = \begin{cases} \frac{5\delta_m - 2\delta_0}{3} + \frac{2(\delta_0 - \delta_m)\rho}{3\rho_{m0}}, & 0 < \rho \leq 2.5\rho_{m0} \\ \delta_0 \exp[-0.01(\rho/\rho_{m0} - 2.5)], & \rho > 2.5\rho_{m0} \end{cases} \quad (\text{A.3})$$

where δ_0 is considered to be uniformly distributed between 122 to 152 m, and $\delta_m = \delta(\rho_{m0})$ is considered to be equal to 122 m.

Once the above model parameters (i.e., the ratio of the radial velocity U_r to tangential velocity U_θ , γ ; the radius ρ_{m0} to the maximum tangential velocity at a specified height z_0 ; the linear variation of ρ_m with height as specified by the slope S ; the reference boundary layer thickness δ_0 ; the reference rotational velocity $u_{r,0}$; the translational speed U_T ; and the tornado path width W) are known, the remaining tasks for defining the wind field in the horizontal plan are to provide equations for predicting the tangential velocity U_θ , the radial velocity U_r , and the rotational velocity $U_{r,\theta}$ at location defined by radial distance ρ and height z . The suggested equations for these velocities are,

$$U_\theta(\rho, z) = U_0 \frac{m(\rho)}{\rho} G(\rho, z) \quad (\text{A.4a})$$

$$U_r(\rho, z) = \gamma' U_0 \frac{m(\rho)}{\rho} F(\rho, z) \quad (\text{A.4b})$$

and

$$U_{r,\theta} = (U_r^2 + U_\theta^2)^{1/2} \quad (\text{A.4c})$$

In the above equation, $m(\rho)$ represents the horizontal variation of tangential and radial wind fields is given by

$$m(\rho) = \begin{cases} \rho_m \left[1 - \exp\left(-1.25643(\rho/\rho_m)^2\right) \right], & 0 \leq \rho < \rho_m \\ A\rho + B, & \rho_m \leq \rho < \rho_0 \\ 0, & \rho > \rho_0 \end{cases} \quad (\text{A.5a})$$

where the parameters A and B describe the rate at which the vortex vanishes outside of the core and are to be determined based on U_{\max} and tornado path width W (see discussion below) and,

$$\rho_0 = \begin{cases} -B/A, & A < 0 \\ \rightarrow \infty, & A \geq 0 \end{cases} \quad (\text{A.5b})$$

$G(\rho, z)$ representing the variation of tangential wind velocity is given by,

$$G(\rho, z) = \begin{cases} 1 - \exp[-\alpha(z + \zeta)/\delta(\rho)], & z \leq \delta(\rho) \\ 1 - \exp[-\alpha(\delta(\rho) + \zeta)/\delta(\rho)], & z > \delta(\rho) \end{cases} \quad (\text{A.6})$$

where the parameter ζ represents an effective sublayer thickness equals 7.62 m and $\alpha =$

10. The function $F(\rho, z)$ representing the variation of the radial velocity is given by,

$$F(\rho, z) = \begin{cases} (z + \zeta) \exp[-\alpha(z + \zeta)/\delta(\rho)]/\delta(\rho), & z \leq \delta(\rho) \\ 0, & z > \delta(\rho) \end{cases} \quad (\text{A.7})$$

Other parameters for Eq. (A.4) are,

$$\gamma' = \gamma \frac{G(\rho_{m0}, z)}{F(\rho_{m0}, z)}, \quad (\text{A.8a})$$

$$\gamma = \frac{|U_r(\rho_{m0}, z)|}{|U_\theta(\rho_{m0}, z)|}, \quad (\text{A.8b})$$

$$U_0 = \frac{U_{r\theta}(\rho_{m0}, z_0)}{m_0 G(\rho_{m0}, z_0) \sqrt{1 + \gamma^2}}, \quad (\text{A.8c})$$

$$m_0 = m(\rho_{m0})/\rho_{m0}, \quad (\text{A.8d})$$

and

$$U_{r\theta}(\rho_{m0}, z_0) = U_{\max} - U_T \quad (\text{A.8e})$$

Parameters A and B and the wind field boundary are determined by making the model compatible with tornado wind profile and the width. Tornado path width W is defined as the distance between the points where the horizontal velocities equal to the reference wind speed v_b , at elevation z_0 .

More specifically, the boundaries of the tornado are determined as follows. Note that there are two cases that need to be considered in determining the left boundary distance from the tornado vortex center, B_l . In the first case which is depicted in Figure A.1a, the horizontal wind speed at ρ_{m0} on the left boundary, denoted by $V_l(\rho_{m0}, z_0)$, is considered to be greater than v_b . In such a case, B_l , B_r , A and B are determined by solving the following equations,

$$W = B_r + B_l, \quad (\text{A.9a})$$

$$m_0 = A + B / \rho_{m0}, \quad (\text{A.9b})$$

$$V_l(B_r) = \left[(U_\theta(B_l, z_0) - U_T)^2 + U_r^2(B_l, z_0) \right]^{1/2} = v_b, \quad (\text{A.9c})$$

and

$$V_r(\rho_r) = \left[U_r^2(\rho_r, z_0) + U_\theta^2(\rho_r, z_0) \right]^{1/2} + U_T = v_b. \quad (\text{A.9d})$$

where ρ_r is the radial distance from the tornado vortex center to the point of intersection between the right boundary and wind field, which is given by,

$$\rho_r = B_r / \cos \beta \quad (\text{A.10a})$$

and,

$$\beta = \tan^{-1} \gamma \quad (\text{A.10b})$$

Since these equations are nonlinear equations, they need to be solved by iteration. For example, one could solve the equations by taking an initial value of $R_l = \rho_{m0}$ and increasing it until the set of equations is satisfied.